A NEW DATA ROTATION SYNCRHONIZATION SCHEME FOR CP BASED OFDM SYSTEMS

SHI MIAO

NATIONAL UNIVERSITY OF SINGAPORE

2003

A NEW DATA ROTATION SYNCRHONIZATION SCHEME FOR CP BASED OFDM SYSTEMS

SHI MIAO

(*B. ENG, XIDIAN UNIVERSITY*)

A THESIS SUBMITTED

FOR THE DEGREE OF MASTER OF ENGINEERING DEPARTMENT OF

ELETRICAL AND COMPUTER ENGINEERING

NATIONAL UNIVERSITY OF SINGAPORE

2003

ACKNOWLEDGMENT

I would like to take this opportunity to express my greatest and most sincere gratitude to my supervisor Associate Professor C.C. Ko for his invaluable guidance, support, and encouragement during my study and research work at National University of Singapore. I would like to thank him for introducing me to the world of wireless communications and teaching me not only in a particular research topic, but also the way to do research works. There is always time for questions and discussions, no matter if they are about details in a basic concept in signal processing or about some ideas in my research work.

I would also like to express my deepest appreciation for my family and friends for their unconditional love and continual encouragement. Without all these, I would have never gotten to where I am today.

Last but not least, I would like to express my gratefulness to the National University of Singapore for granting me the Research Scholarship without which I could not have carried out my research work.

ABSTRACT

In this thesis, we present a new data rotation scheme for symbol timing and carrier frequency offset (CFO) estimation of orthogonal frequency-division multiplexing (OFDM) systems. We first analyze Beek's cyclic prefix (CP) based joint ML estimator [2] and find that its performance can be improved when the average energy of the CP increases. We then propose a new data rotation scheme, where we intentionally introduce a cyclic shift after the inverse fast Fourier transform (IFFT) in the transmitter, to obtain a higher energy CP. This cyclic shift will not impair the orthogonality among the subcarriers and its recovery can be combined with channel estimation in the receiver. We analyze the performance of the new data rotation scheme by using order statistics theory. Our results shows that the new scheme can provide a 1.6dB gain in the performance of the frequency offset estimator and a 6dB gain for the timing estimator at 15dB SNR.

Keywords: OFDM, ICI, ISI, FFT, CP, ML

TABLE OF CONTENTS

LIST OF FIGURES

LIST OF TABLES

SUMMARY

Orthogonal frequency-division multiplexing (OFDM) systems are highly sensitive to frequency and timing offset errors [1-4]. Most OFDM time-frequency offsets estimators proposed in the literature require pilot symbols or training sequences. As presented in [5-8], synchronization can be achieved by transmitting pilot symbols. This wastes bandwidth, especially in broadcast systems where the transmitter would have to keep transmitting pilot symbols periodically to allow new users to synchronize. In [5], the null subcarriers in OFDM symbols are used for the estimation of the carrier frequency offset (CFO). The performance of the estimation depends on the number of the null subcarriers and can be affected by symbol timing offsets.

Apart from these methods, several cyclic prefix (CP) based blind synchronization schemes that use only the transmitted symbol statistics for symbol synchronization have also been proposed [6-9]. These exploit the redundancy in the CP, and do not require additional pilot symbols.

In this thesis, we present a new data rotation scheme to improve the performance of CP based blind synchronization schemes [6-9]. The new scheme is based on data rotation and makes use of the following useful properties of fast Fourier transform (FFT). Essentially, if we introduce a cyclic shift of u samples for the transmitted signal $x(n)$ after inverse fast Fourier transform (IFFT), the orthogonality among the subcarriers will not be affected. Instead, this intentionally introduced cyclic shift will result in a phase rotation at each subcarrier in the receiver after FFT. In pilot based coherent modulation systems, this phase rotation can be compensated for by a frequency-domain channel equalizer [9-11]. As a result, we can cyclically

shift or rotate the OFDM symbol after IFFT and assign the CP in such a way to improve the performance of the joint maximum-likelihood (ML) estimator [5]. Specifically, based on the analysis of Beek's joint ML estimator [5], we find that the transmitted signal will have a better synchronization performance if we rotate or shift the OFDM symbol to give rise to a higher energy CP for the symbol.

Therefore, in the new data rotation scheme, a cyclic shift after IFFT in the transmitter is intentionally introduced to obtain a higher energy CP. This cyclic shift does not impair the orthogonality among the subcarriers, and its recovery can be combined with channel estimation in the receiver [9-11]. As a result of the increase in the energy of the CP, however, the new scheme can provide a 1.6dB gain in the performance of the CFO estimator and a 6dB gain for the timing estimator at 15dB SNR.

Chapter 1

Introduction

This chapter first provides a quick overview of the orthogonal frequency division multiplexing (OFDM) technology. It then introduces the application of OFDM in various communication areas. Following which, the synchronization problem in OFDM systems, which is the main task of this thesis, is presented. Lastly, this chapter concludes with the organization of this thesis.

1.1 Introduction of OFDM

A central problem in communications is reliably and efficiently transmitting information signals over imperfect channels. One successful approach to achieve high-speed data transmission is multicarrier modulation (MCM), also called multitone modulation [1]. The principle of MCM is to divide the transmission channel into a number of orthogonal subchannels or subcarriers.

The main advantage of MCM over a conventional single carrier modulation is its robustness of data transmission over multipath channels. This feature of MCM allows for system designs supporting high data rates while maintaining symbol durations much longer than the memory of the channel. As a result, we avoid complex channel equalization.

Another advantage of this parallel modulation technique is its reduced susceptibility to various forms of impulse noise.

The earliest MCM modem techniques borrowed from conventional frequency division multiplexing (FDM), and used filters to completely separate the bands. The power spectral density (PSD) of a FDM signal with just 5 sub-bands is shown in Fig. 1.1. Because of the difficulty of implementing very sharp filters, each of the signals must use a bandwidth, $(1+\alpha)f_s$, $(\alpha > 0)$, which is greater than the Nyquist minimum, f_s, where α is the parameter related to the efficiency of band usage, which is given by, $f_s / f = 1/(1+\alpha)$.

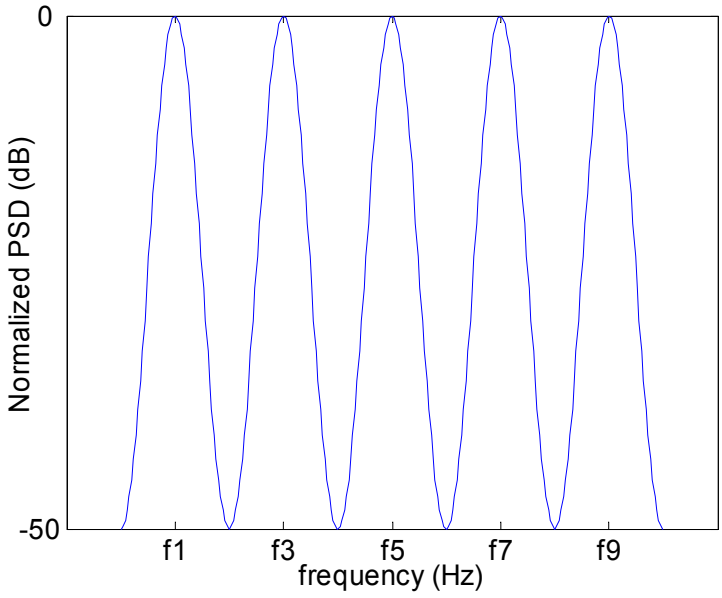

Fig. 1.1 Power spectral density of a FDM signal when $\alpha = 1$.

To improve the bandwidth efficiency, a discrete Fourier transform (DFT) based MCM scheme, OFDM, was later proposed [1-3]. Among many possible implementational schemes, the FFT based OFDM with cyclic prefix (CP) is of

particular interest because of the high bandwidth efficiency and less complexity. Fig. 1.2 shows the PSD of an OFDM signal using rectangular pulse shape. Note that each subcarrier is spaced orthogonally as closely as possible in frequency, and the spectrum of each subcarrier overlaps with its adjacent subcarriers, which is different from the spectrum of FDM in Fig. 1.1.

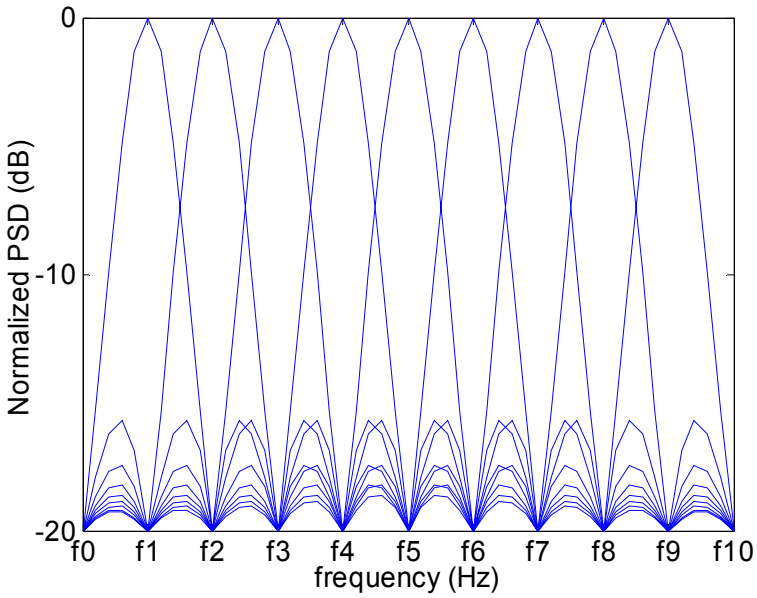

Fig.1.2 PSD of an OFDM signal using rectangular pulse shape.

Therefore, OFDM is an effective technique for combating multipath fading and for transmitting high-bit-rate data over mobile wireless channels.

1.2 Applications of OFDM

With the advances in digital signal processing (DSP) and very large scale integration (VLSI) technologies, discrete time implementations are now used extensively. They have facilitated the adoption of OFDM by overcoming earlier problems of high-speed memory and large computation.

The inherent potential of OFDM was utilized in the design of wireline DMT modems for xDSL/ADSL applications pioneered in the 1980s and being deployed recently in the United States [27]. These latter systems applied adaptive loading and modulation theory to practical high speed Internet access and enabled local telephone companies to leverage copper wire infrastructure.

Also, OFDM is being considered for several wireless LAN standards [3]. For example, IEEE 802.11a and 802.11g wireless LAN (WLAN) standards offer theoretical maximum speeds of 54 Mbits per second, with real-world data rates of up to 22 Mbps. This is higher than the rates produced by previous WLAN technologies such as IEEE 802.11b. The European Telecommunications Standards Institute's proposed Hiper-LAN2 (high-performance radio LAN 2) and Japan's Mobile Multimedia Access Communications broadband WLAN technologies also use OFDM. In addition to WLANs, vendors like Flarion Technologies and NextNet Wireless are using OFDM to bring higher speeds to fixed-wireless metropolitan area networks (MANs).

While OFDM scheme has obtained more and more interests, several problems may limit the technology's broad usefulness and widespread adoption. Among them, synchronization is one of the most important tasks to be solved at the receiver.

1.3 Background of synchronization problems in OFDM systems

Synchronization of an OFDM signal requires determining the parameters of symbol timing offset, carrier frequency offset, and phase noise [19]. Since the phase noise does not impair the orthogonality between the subcarriers of OFDM systems and can be easily estimated and corrected using pilot samples inserted in the OFDM

symbol, in this thesis, we will mainly discuss the other two synchronization parameters.

1.3.1 Carrier frequency offsets and ICI

According to the above sections, one of the main reasons that OFDM has obtained more and more interests is its high spectral efficiency compared with other MCM implementation schemes. In order to attain this high spectral efficiency, OFDM carriers have orthogonal overlapping spectra as compared with well known frequency division multiplexing (FDM). The first side lobe is only 13 dB down from the peak at the desired subcarrier. Hence, a frequency offset may cause considerable ICI coming from other subcarriers.

Therefore, OFDM systems are very sensitive to inaccurate frequency references or frequency dispersion due to carrier frequency drifts and other environmental variations [5-25]. In this thesis, we will mainly consider the effect of the inaccurate frequency references, that is, the frequency difference in the oscillators between the transmitter and the receiver.

The impact of the carrier frequency offset (CFO) is the loss of subcarrier orthogonality, which introduces ICI and severely degrades the system performance [5-25]. The estimation of carrier offset from noisy data is a major task to mitigate unwanted ICI in OFDM. It is necessary to have high performance estimators that will reduce the uncompensated frequency offset to a small fraction of the subchannel signaling rate. The sensitivity to carrier frequency offset is widely acknowledged as one of the major disadvantages of OFDM. Accurate carrier offset estimation and

compensation is more critical in OFDM than in other modulation schemes [5-25]. For a free running receiver local oscillator, the system performance rapidly deteriorates when the carrier frequency offset between transmitter and receiver is greater than a small fraction of the intercarrier spacing. Therefore, it is necessary to estimate carrier offset at the receiver with high resolution.

1.3.2 Symbol timing offsets and ISI

In OFDM systems, a CP has been inserted before the data part of the OFDM symbol to alleviate the ISI problems. We assume that the length of the channel impulse response is less than the length of the CP. In the receiver side, an ISI free symbol can be obtained by removing the CP part affected by the multipath. However, when the estimation of the symbol start position is not accurate, there will be a timing offset leading to ISI between the adjacent symbols.

The purpose of the symbol timing offset is to find the correct position of the FFT window, which contains samples of one OFDM symbol. That is, the samples inside the FFT window will not include samples of either earlier or later symbols.

1.4 Contribution of this thesis

In this thesis, we present a new data rotation scheme to improve the performance of CP based blind synchronization schemes [5-24]. In this new scheme, a cyclic shift after IFFT in the transmitter is intentionally introduced to obtain a higher energy CP. This cyclic shift does not impair the orthogonality among the subcarriers, and its recovery can be combined with channel estimation in the receiver [9-11]. As a result of the increase in the energy of the CP, the new scheme can provide a 1.6dB

gain in the performance of the CFO estimator and a 6dB gain for the timing estimator at 15dB SNR.

1.5 Notations

Throughout this thesis, the following notations are used. We use bold faced capital letters, $\mathbf{X}$, $\mathbf{Y}$, …, to denote matrices or vectors. The lower case italic English letters are to denote scalar values, such as x, y, ….

The symbol $\mathbf{A}^T$ denotes the transpose of $\mathbf{A}$, and the symbol $\mathbf{A}^H$ denotes the complex conjugate transpose of $\mathbf{A}$.

1.6 Thesis Outline

This thesis is organized as follows:

In Chapter 2, we first provide the diagram of the OFDM systems. The two main synchronization problems, symbol timing offset and the CFO, are discussed in detail and analyzed by giving their mathematical models. After reviewing the present synchronization schemes proposed in OFDM systems [5-25], we compare the different schemes and focus our thesis on the CP based synchronization schemes in OFDM systems. Synchronization schemes in IEEE 802.11a standard are also mentioned and introduced.

In Chapter 3, based on the analysis of the synchronization problems in OFDM systems, and assuming that the statistics of the OFDM transmitted signals are additive white Gaussian noise (AWGN), the CP based Maximum Likelihood (ML) synchronization scheme proposed by Beek is already introduced in [5]. Following

which, the performance of Beek's joint estimator [5] is analyzed in detail. We investigate the symbol timing offset errors of $+1$, -1 and m, $m \neq 1$ samples, respectively. Under perfect estimation of symbol timing offset, we provide a closed-form expression for the performance of the CFO estimator.

In Chapter 4, applying the analysis of the last chapter and an interesting feature of FFT, we present the new data rotation scheme for the joint estimation of symbol timing and the CFO. The implementation of this scheme on both transmitter and receiver under IEEE 802.11a WLAN is also presented.

In Chapter 5, first, we give the mathematical analysis of the performance improvement of the CFO estimator by applying order statistics. Based on this, a closed form formula for the SNR gain in the CFO estimation is followed. By introducing the expectation of the timing metric and its influence on the timing estimator, we also investigate the performance improvement of the symbol timing estimator by using the new data rotation scheme.

In Chapter 6, simulation results are given to prove the theoretical analysis given in the previous chapters and to illustrate the performance of the new method.

In Chapter 7, we conclude this thesis and propose some future works.

Chapter 2

OFDM System and Synchronization Problems

This chapter is to further the introduction of Chapter 1 by providing the theoretical background of the OFDM system and its synchronization problems. We start this chapter with the mathematical model of the OFDM system. The symbol timing and CFO synchronization problems have also been analyzed in detail and the mathematical expression of both are obtained. A general review of the recent works on this topic is presented. Last, we introduce the synchronization issues in IEEE 802.11a standard.

2.1 OFDM System Overview

As shown in the system block diagram of Fig.2.1, we consider an OFDM system that uses a FFT of size N. The transmitted signal $s(n)$ is generated using an IFFT on N QAM symbols $X(k)$, where n is the time index and k is the subcarrier index.

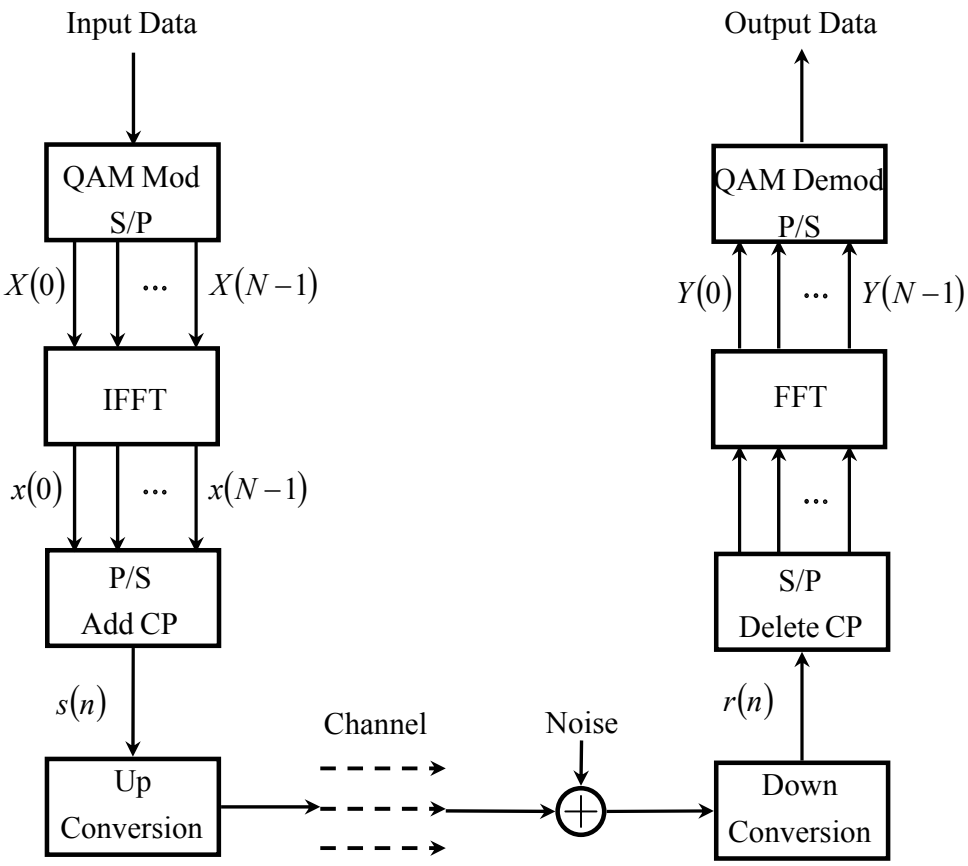

Fig.2.1 Block diagram of OFDM System

To prevent ISI, a CP of g samples is placed before the data portion of the signal. If g is larger than the maximum delay of the channel impulse response (CIR) L, the orthogonality of the system is preserved even in the presence of multipath. Mathematically, the signal after IFFT is given by [26]

$$x(n)=\frac{1}{\sqrt{N}}\sum_{k=0}^{N-1}X(k)e^{\frac{j2\pi nk}{N}},\ 0\le n\le N-1. \tag{2-1}$$

After adding the CP, the transmitted baseband signal of the current OFDM symbol is

$$s(n)=\begin{cases} x(n+N-g), & 0 \le n < g \\ x(n-g), & g \le n < N+g \end{cases}. \tag{2-2}$$

The received signal after transmission through the multipath channel is given by

$$r(n)=\sum_{l=0}^{L-1} s(n-l)h(l)+w(n), \tag{2-3}$$

where $h(n)$ is the sampled channel impulse and $w(n)$ is the corrupting AWGN with variance σ_w^2. By correctly removing the CP, the signal can be demodulated using a FFT. The received signal after FFT is

$$Y(k)=X(k)H(k)+W(k), \tag{2-4}$$

where $W(k)$ is the complex white Gaussian noise after FFT and

$$H(k)=\sum_{l=0}^{L-1} h(l)e^{\frac{-j2\pi kl}{N}} \tag{2-5}$$

is the channel transfer function.

2.2 Carrier frequency offset

In the above subsection, ideal synchronization in the OFDM receiver has been assumed. However, this is not always the case. There is usually a frequency offset due to the mismatch of the oscillators in the transmitter and the receiver. Denote Δf as the difference in frequency between the transmitter and receiver oscillator. The normalized frequency offset ε is given by

$$\varepsilon = NT\Delta f \ , \tag{2-6}$$

where N is the size of FFT and T is the sampling period. Due to the effect of the carrier frequency offset ε, the received sequence given in (2-3) will be changed to

$$r(n) = e^{j\frac{2\pi n\varepsilon}{N}} \sum_{l=0}^{L-1} s(n-l)h(l) + w(n), \tag{2-7}$$

The CFO is modeled in [13] as a complex multiplicative distortion of the received data in the time domain given by $e^{j2\pi\varepsilon n/N}$. Consequently, the output of the k th subcarrier after FFT is modeled as

$$Y(k) = \sum_{n=0}^{N-1} e^{-j\frac{2\pi nk}{N}} e^{j\frac{2\pi n\varepsilon}{N}} \sum_{l=0}^{L-1} s(n-l)h(l) + W(k). \tag{2-8}$$

Specifically, when the carrier frequency offset ε is an integer multiple of the subcarrier spacing, the above equation is simplified as

$$Y(k) = X(k+\varepsilon)H(k) + W(k). \tag{2-9}$$

In this case, the effect of the CFO does not impair the orthogonality among the subcarriers. Thus, it is easy to be compensated after FFT with the aid of pilots inserted in the transmitted OFDM symbols [9-14].

Generally, the CFO will have a fractional part θ_f. The output of the k th subcarrier after FFT is given in [13]

$$Y(k) = X(k)\frac{\sin(\varepsilon)}{N\sin\left(\frac{\pi\varepsilon}{N}\right)} + \sum_{n=0,n\neq k}^{N-1} X(n)\frac{\sin(n+\varepsilon)}{N\sin\left(\frac{\pi(n+\varepsilon)}{N}\right)} . \quad (2\text{-}10)$$

The second term in the right hand side (RHS) of the above equation is the ICI contributed by other subcarriers. The orthogonality of the system is destroyed. Considering the damaging impact of the fractional part of the CFO, in this thesis, we will only concern this part of the CFO.

Based on the above analysis, techniques in [5-9] employing cyclostationarity in the OFDM symbols as a result of adding the CP, have been proposed to estimate the CFO. Specifically, without considering the impact of AWGN, there will be some pairs of correlated received signals separated with N samples that satisfy

$$\frac{r(n)}{r(n+N)} = e^{-j2\pi\varepsilon} . \quad (2\text{-}11)$$

2.3 Timing offset

Apart from CFO, there also may be a timing offset caused by the misalignment of the FFT window and the received symbol. Usually, the timing synchronization can be implemented in two steps: coarse and fine timing synchronization.

Coarse timing synchronization can be obtained by calculating the correlation for the training symbols and the received signal continuously. Specifically, in the packet based IEEE 802.11a standard, two preambles in the beginning of each OFDM packet are

well suited for this purpose. In this thesis, we assume the coarse synchronization has been obtained and the residual timing offset is within the range of one OFDM symbol.

As shown in Fig. 2.2, this residual timing offset may occur in two situations depicted in [13].

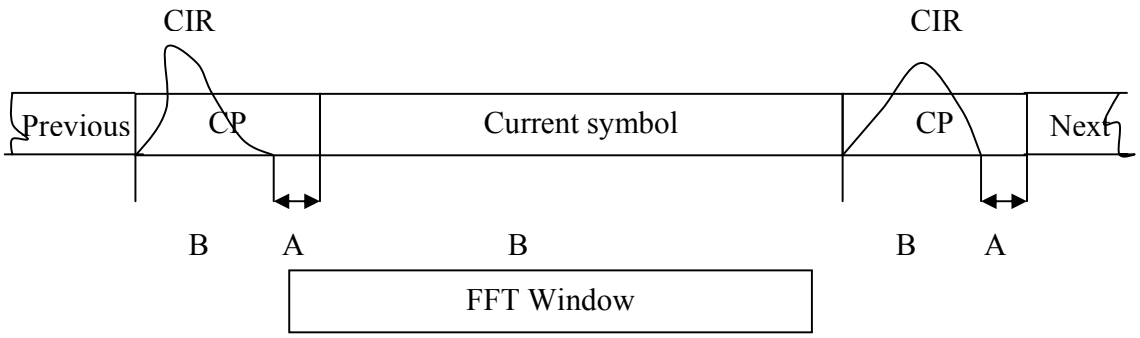

Fig. 2.2 Principle of timing synchronization.

As can be seen, as long as the start position of the FFT window is within region A, no ISI occurs. The only effect suffered by the subchannel symbols is a change in phase that increases with the subcarrier index according to

$$Y(k) = X(k)H(k)e^{-j\frac{2\pi\theta}{N}} + W(k). \tag{2-12}$$

This change in phase will not impair the orthogonality among the subcarriers and can be compensated by using a frequency domain equalizer.

If the start position is within region B, the subcarrier symbols are given by [13]

$$Y(k)=\frac{N-\tau}{N}X(k)H(k)e^{-j\frac{2\pi\theta}{N}}+W_{\tau}(k)+W(k), \tag{2-13}$$

where the second term in the RHS, $W_{\tau}(k)$ is the extra noise introduced by the ISI.

Similarly, normalized by the sampling period, the timing offset can be divided into an integer part θ_0 and a fractional part θ_f. [12] shows that, in an ideal rectangular pulse shaping system, the fractional part θ_f results in phase offsets which can be corrected through simple phase rotation. However, the integer part θ_0 can not be so easily corrected and will be the concern of this thesis.

Therefore, assuming that the FDE is used, the main task of the synchronization scheme in OFDM systems will be the reduction of ICI and ISI. That is, the main task of the synchronization schemes is to remain the orthogonality among the subcarriers.

2.4 Synchronization schemes in OFDM systems

Generally, the existing parameter estimation techniques for synchronization of OFDM systems can be classified into two main subclasses: schemes that are implemented in the time domain and schemes that are implemented in the frequency domain. Since the former will cause less delay and the FFT does not have to be calculated before the estimate calculation, most of existing synchronization schemes are executed in the time domain.

The time domain estimation techniques for synchronization of OFDM systems can also be classified into two main subclasses: minimum mean-square-error (MMSE) and maximum-likelihood (ML) estimators. In the MMSE approach, the estimator uses information provided by the reference signals (pilot tones or null subchannels) in order to minimize a cost function associated with the synchronization parameters [12-17]. A salient feature of this approach is that no probabilistic assumptions are made about the data. Also, due to their inherent characteristic, MMSE estimators usually result in a tractable (globally stable) and easy to implement realization. However, MMSE estimators do not necessarily result in an unbiased and minimum variance estimate of the unknown parameter. On the other hand, classical probabilistic approaches, such as ML or MVU estimators, estimate the unknown parameter, subject to minimum probability of error or minimum variance criteria [5-11]. Although not exactly efficient, ML estimators are asymptotically MVU. That is, their variance approaches that of MVU estimator as the length of data record increases.

Besides the above synchronization schemes, Zhao and Haggman [24] proposed a simple but efficient way of suppressing ICI in OFDM systems. In this method each data symbol is modulated onto one pair of subcarreirs by using the original signal and the signal multiplied by -1. By doing so, the ICI signals generated with a pair of subcarriers can be self cancelled each other. However, the self ICI cancellation scheme requires a tracking step for higher fractional frequency offset values and reduces bandwidth efficiency by a factor of 2.

To avoid the reduction of bandwidth efficiency, a ML CP based blind synchronization scheme was introduced by Beek [5]. In this approach, the additional information provided by the CP is used to obtain the likelihood function for joint estimation of symbol timing error and frequency offset in an OFDM system. The analysis presented in this thesis reveals that the performance of this scheme can be improved by changing the statistic of the transmitted signal using our new proposal.

2.5 Synchronization in IEEE 802.11a

In 1999 the IEEE 802.11a standard for WLAN was established [27]. Until recently it has mainly been used in USA, but it is now coming to other parts of the world. The radio interface is packet based and uses OFDM to achieve high data rates. Since OFDM is rather strict when it comes to synchronization, several techniques are dedicated in IEEE 802.11a standard for this use.

The IEEE 802.11a MAC (Medium Access Unit) unit uses a technique called carrier sense multiple access collision avoidance (CSMA/CA). The transmitter first listens to see if anyone is transmitting. If this is not the case it sends a short request-to-send package containing, among other things, the length of the unsent packet. The transmitter waits for the response before it starts transmitting. Other transmitters within reach also receive the request-to-send packet and then know how long the transmission will take.

The structure of the OFDM symbol in IEEE 802.11a standard is also designed to use for the synchronization issues. In IEEE802.11a, the radio transmission takes place in a 20 MHz wide frequency band divided into 64 sub bands. 48 of these sub bands are used for transmission. Since the IEEE 802.11 receiver is coherent, which means that the phase has to be estimated before the decoding takes place, four pilot subcarriers are inserted in each OFDM symbol estimate the phase. The remaining 12 sub bands are unused.

In the table below are some of the timing related parameters from the IEEE 802.11a standard [27].

Parameter	Value
N_{SD} : Number of subcarriers	48
N_{SP} : Number of pilot subcarriers	4
N_{ST} : Number of subcarriers in total	52
f_S : sampling frequency	20 M samples/s
Subcarrier frequency spacing	0.3125 MHz
T_{FFT} : IFFT/FFT time	3.2 μs
T_{GI} : GI duration	0.8 μs
T_{GI2} : Training symbol GI duration	1.6 μs

Table 2.1 Timing related parameters in IEEE802.11a.

To detect the correct timing start position and frequency offset, IEEE 802.11a use 10 short preambles and 2 long preambles to obtain the synchronization of the frequency

and timing parameters. Each IEEE 802.11a packet is preceded by a preamble, a sequence of samples whose purpose is to allow detection, synchronization and training. The standardized preamble structure, in the time domain, is shown to the left in Fig. 2.3.

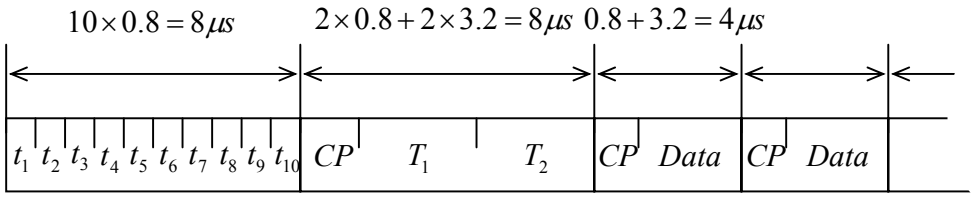

Fig. 2.3 IEEE802.11a OFDM preamble structure

As can be seen, the first half of the preamble consists of ten identical short symbols t_i, $i = 1,\cdots,10$. Each short symbol consists of 16 samples. The second half of the preamble consists of two identical long symbols T_1 and T_2, each of which is 64 samples long, preceded by a 32 sample CP. The symbols are designed so that the correlation between two subsequent samples is minimal.

In [27], a 4-6 sample shift is presented as a rule of thumb for the maximum tolerable symbol timing error in an IEEE802.11a system.

The standard specifies a maximum oscillator frequency error of 20 ppm (parts per million) of the carrier frequency. If the transmitter and receiver have errors with inverse signs the observed total error will be 40 ppm. If a carrier frequency of approximately 5.3 GHz is assumed, this translates to a $\Delta f_{\max}$ that is 212 kHz.

Using it can be seen that for a 0.1 dB degradation, the maximum CFO is about 1% of the distance between the subcarriers or about 0.58 ppm. This will be used as a rule of thumb for the maximum tolerable CFO error.

Chapter 3

Analysis of Beek's ML Estimator

Based on the analysis of the synchronization problems in the previous chapter, in this chapter, we investigate the well known blind ML synchronization scheme proposed by Beek [5]. The factors affect the performance of this joint CP based timing and CFO estimation method have also been analyzed in detail.

3.1 ML estimator proposed by Beek

Assuming that the channel is non-dispersive and the transmitted signal is only affected by AWGN, Beek proposed a method for jointly estimation of the symbol timing and CFO through the use of ML technique [5]. Following this approach, the uncertainty in the arriving time of the OFDM symbol is modeled as a delay in the channel impulse response, that is

$$h(n) = \delta(n - \theta_0), \tag{3-1}$$

where θ_0 is the timing offset in the receiver caused by unknown arriving time of the symbol. This is illustrated in Fig.3.1, where we take $r(0)$ as the first sample of the current symbol while the actual true timing start is $r(\theta_0)$.

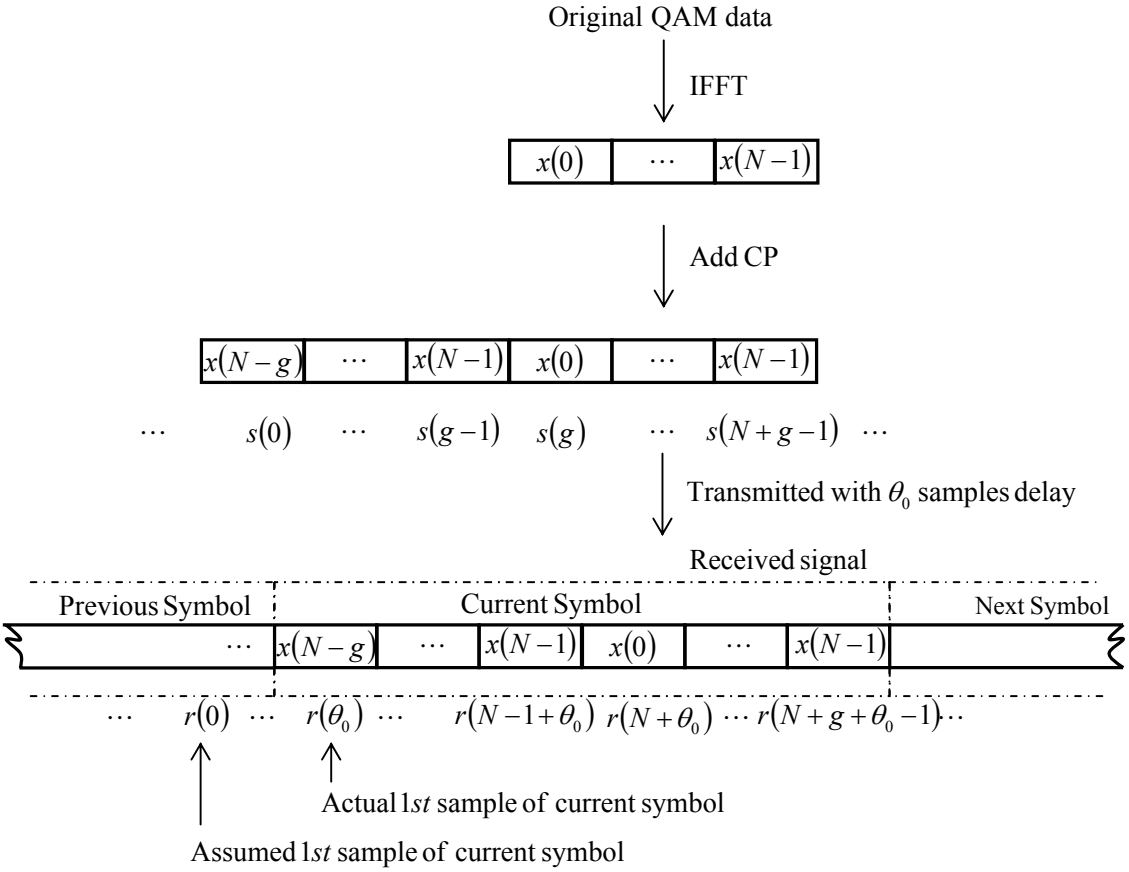

Fig. 3.1 OFDM symbol transmission through the channel $h(n)=\delta(n-\theta_0)$.

With the assumption that the size of the IFFT N is large, the transmitted signal after IFFT can be approximated as white Gaussian [5]. Therefore, after adding the CP,

using (2-6) and taking AWGN into consideration, the correlation between $r(n)$ and $r(n+m)$ is

$$\mathrm{E}\left[r(n)r^*(n+m)\right]=\begin{cases}\sigma_s^2+\sigma_w^2 & m=0\\ \sigma_s^2 e^{-j2\pi\varepsilon} & m=N\\ 0 & otherwise\end{cases},\ n=\theta_0,\cdots,(\theta_0+g), \tag{3-2}$$

where $\sigma_s^{\,2}$ is the signal power.

Taking an observation vector of $(2N+2g-1)$ received samples, the joint ML estimator presented by Beek in [5] for the symbol timing start position θ and the CFO ε is given by

$$\hat{\theta}=\arg\max_{\theta}\left[f(\theta)\right] \tag{3-3}$$

and

$$\hat{\varepsilon}=-\frac{1}{2\pi}\angle\left[\gamma\left(\hat{\theta}\right)\right], \tag{3-4}$$

where

$$f(\theta)=|\gamma(\theta)|-\rho\phi(\theta), \tag{3-5}$$

$$\gamma(m)=\sum_{n=m}^{m+g-1}r(n)r^*(n+N), \tag{3-6}$$

$$\phi(m)=\sum_{n=m}^{m+g-1}|r(n)|^2+|r(n+N)|^2, \tag{3-7}$$

and

$$\rho = \frac{\sigma_s^{\,2}}{2\left(\sigma_s^{\,2} + \sigma_w^{\,2}\right)}. \tag{3-8}$$

3.2 Analysis of Beek's scheme

We will now presents an analysis of the joint CP based timing and CFO estimation method outlined above [5]. We will first discuss the factors that affect the performance of the timing offset estimator, following by giving some comments on the performance of the CFO estimator.

3.2.1 Performance of symbol timing offset estimation

From (3-3), a symbol timing synchronization error occurs when

$$\chi_\theta = f(\theta) - f(\theta_0) > 0,\ \theta \neq \theta_0. \tag{3-9}$$

Specifically, a timing error of $+1$ sample occurs when

$$\chi_{\theta_0+1} = f(\theta_0 + 1) - f(\theta_0) > 0. \tag{3-10}$$

In Appendix A, for the case of high SNR, it is shown that χ_{θ_0+1} is given by

$$\chi_{\theta_0+1} = -\frac{1}{2}\left|s_+ - v_+\right|^2 + \frac{1}{2}\left|v_+\right|^2, \tag{3-11}$$

where

$$s_+ = s(g) - s(N+g) \tag{3-12}$$

and

$$v_+ = e^{j\psi_0}\left[w^*(\theta+g) - e^{j2\pi\varepsilon}w^*(\theta+g+N)\right] . \tag{3-13}$$

From (3-11), when χ_{θ_0+1} is larger than zero,

$$\left|s_+ - v_+\right|^2 < \left|v_+\right|^2, \tag{3-14}$$

in which case, a timing error of $+1$ sample will occur. Note that s_+ is the difference between $s(g)$ and $s(N+g)$. As shown in Fig.3.2, $s(N+g)$ is the first sample transmitted in the next OFDM symbol, while $s(g)$ is inside the current OFDM symbol.

Similarly, there may also be a timing error of -1 sample when χ_{θ_0-1} is larger than zero. As shown in Appendix A, when the SNR is high, χ_{θ_0-1} is given by (A-21) or

$$\chi_{\theta_0-1} = -\frac{1}{2}\left|s_- - v_-\right|^2 + \frac{1}{2}\left|v_-\right|^2, \tag{3-15}$$

where

$$s_- = s(-1) - s(N-1) \tag{3-16}$$

and

$$v_- = e^{j\psi_0}\left[w^*(\theta-1) - e^{j2\pi\varepsilon}w^*(\theta+N-1)\right] . \tag{3-17}$$

Likewise, from (3-15), when χ_{θ_0-1} is larger than zero,

$$|s_- - v_-|^2 < |v_-|^2, \tag{3-18}$$

in which case, a timing error of -1 sample will occur. Note that s_- is the difference between $s(-1)$ and $s(N-1)$. As shown in Fig.3.2, $s(-1)$ is the last sample transmitted in the previous OFDM symbol, while $s(N-1)$ is inside the current OFDM symbol.

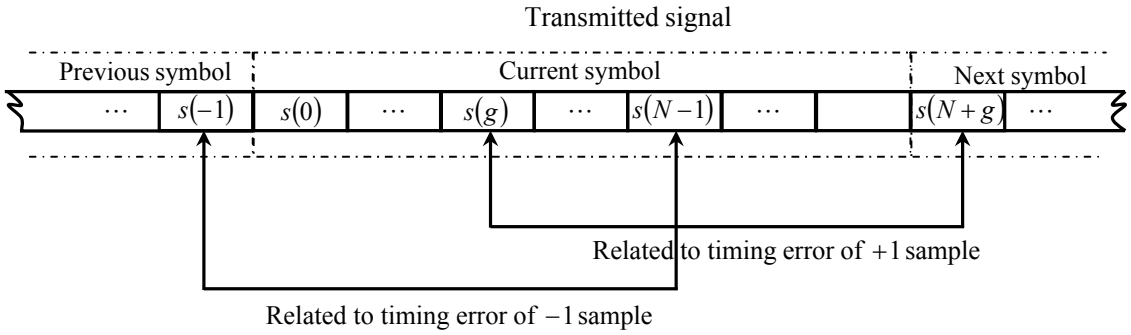

Fig. 3.2 Transmitted OFDM symbols and samples related to the $+1$ and -1 sample timing error.

To show that the value of χ_{θ_0+1} and χ_{θ_0-1} given by (3-11) and (3-15) are quite close to their exact values given by (3-9) when the SNR is high, a comparison is made between the analytical derivations given by (3-11) and (3-15) and the exact values given by (3-9). We denote the deviation of χ_{θ_0+1} in (3-11) from the exact value given by (3-9) as μ_+:

$$\mu_+ = f(\theta_0 + 1) - f(\theta_0) + \frac{1}{2}|s_+ - v_+|^2 - \frac{1}{2}|v_+|^2. \tag{3-19}$$

Similarly, let μ_- denote the deviation of $\chi_{\theta_0 - 1}$ in (3-15) from the exact value given by (3-9):

$$\mu_- = f(\theta_0 - 1) - f(\theta_0) + \frac{1}{2}|s_- - v_-|^2 - \frac{1}{2}|v_-|^2. \tag{3-20}$$

Fig. 3.3 shows the histogram giving the relative frequency of μ_+ and μ_- over 5000 OFDM symbols under the scenario of $SNR = 30$, $N = 64$, $g = 16$, and a timing offset of $\theta_0 = 30$. It is clear that the derivations given by (3-11) and (3-15) for $\chi_{\theta_0 + 1}$ and $\chi_{\theta_0 - 1}$ resemble very closely the exact values given by (3-9).

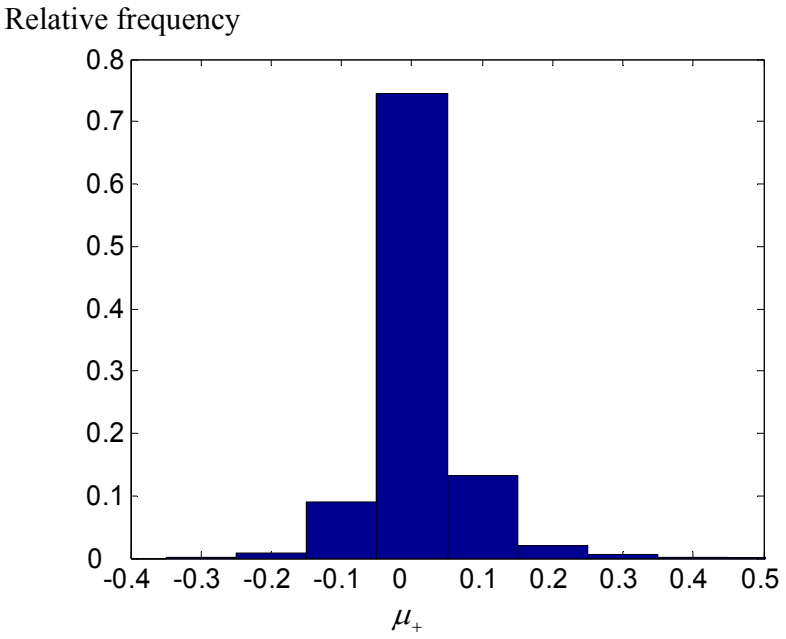

Fig. 3.3 Ralative frequency histogram of (a) μ_+ given by (3-19) and (b) μ_- given by (3-20).

Apart from the timing errors of $+1$ and -1 sample, there are also timing errors of $\left(\hat{\theta}-\theta_0\right)$ samples, where $\left|\hat{\theta}-\theta_0\right|>1$. However, the timing estimate is likely to be around the true timing offset θ_0 especially at high SNR. Fig. 3.4 shows the relative frequency of the timing errors over 5000 OFDM symbols under the scenario of $N=64$, $g=16$, $SNR=10$ dB and $\theta_0=30$. Clearly, the performance of the timing estimator [5] depends mainly on the relative frequency of the timing errors of $+1$ and -1 sample.

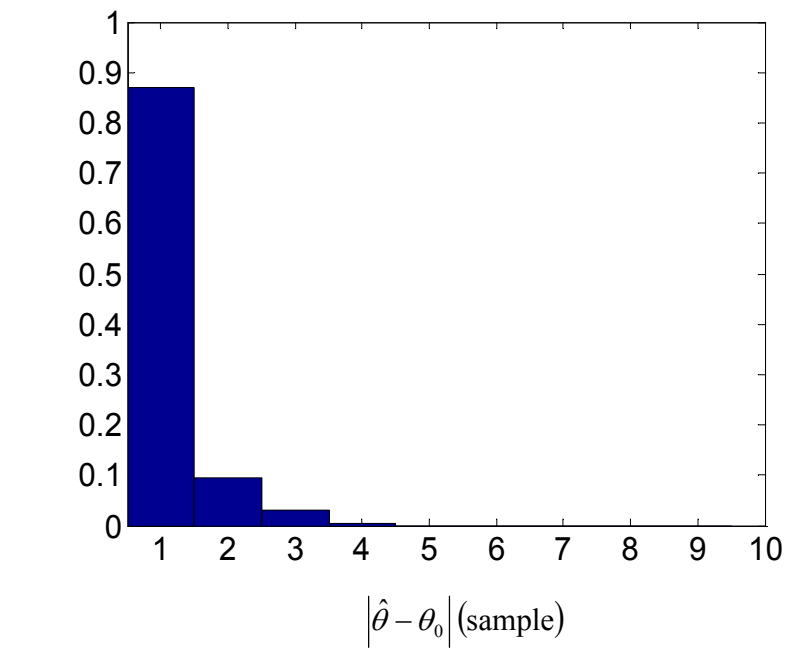

Fig. 3.4 Relative frequency histogram of timing errors of $\left|\hat{\theta}-\theta_0\right|$ samples.

We will now show that a higher energy CP will give rise to a better performance of the timing estimator. Suppose the average power of the CP is $\Delta_{\mathrm{CP}}{}^2\sigma_s{}^2$, where

$\Delta_{\mathrm{CP}}{}^2 > 1$. As shown in Fig. 3.2, $s(N+g)$ and $s(-1)$ are inside the CP of the next and the previous OFDM symbol respectively, while $s(g)$ and $s(N-1)$ are outside the CP. In Appendix B, the expectation of the modulus squares of s_+ and s_- are given by

$$\mathrm{E}\left[|s_{\pm}|^2\right] = \frac{\Delta_{\mathrm{CP}}{}^2(N-2g)+N}{N-g}\sigma_s{}^2. \tag{3-21}$$

The right hand side (RHS) of (3-27) is a monotonically increasing function of $\Delta_{\mathrm{CP}}{}^2$. When the energy of the CP increases or $\Delta_{\mathrm{CP}}{}^2 > 1$, the modulus squares of s_+ and s_- are increased. Assuming the transmitted signal to be independent of the noise in the receiver, an increase in the modulus squares of s_+ and s_- will lead to a decrease in the expectation of χ_{θ_0+1} and χ_{θ_0-1}. As a result, the numbers of $+1$ and -1 sample timing errors are reduced, leading to a better performance in the timing estimator.

3.2.2 Performance of CFO estimation

We will now give some comments on the CFO estimation. Under perfect knowledge of the timing offset error, substituting $\hat{\theta} = \theta_0$ into (3-4) and combining this with (2-3) and (2-6), we get

$$\hat{\varepsilon} = -\frac{1}{2\pi}\arg[\gamma(\theta_0)], \tag{3-22}$$

where

$$\gamma(\theta_0) = e^{-j2\pi\varepsilon}\sum_{n=0}^{g-1}|s(n)|^2 + \sum_{n=0}^{g-1}\left[s(n)w^*(n+N) + e^{-j2\pi\varepsilon}s^*(n)w(n) + w(n)w^*(n+N)\right]. \qquad (3\text{-}23)$$

The first term on the RHS of (3-23) corresponds to the energy of the CP, while at high SNR, the second term on the RHS of (3-23) can be ignored. Clearly, the performance of the CFO estimator also depends on the energy of the CP.

Chapter 4

New Data Rotation Scheme

In this chapter, we will present a new data rotation scheme to improve the performance of the joint ML estimator analyzed in the Chapter 3 [5]. Assuming the phase noise can be corrected in the receiver, we add a maximum energy CP for each OFDM symbol. The implementation of the former in the transmitter and the receiver will be given based on IEEE 802.11a standard [27].

4.1 Circular shift property of the FFT

The new scheme is based on data rotation and makes use of the following useful properties of FFT. Essentially, if we introduce a cyclic shift of u samples for the transmitted signal $x(n)$ after IFFT, the transmitted sequence will be given by

$$s(n)=\begin{cases} x(n+N-g+u), & 0 \le n < g-u \\ x(n-g+u), & g-u \le n < g \\ x(n-g), & g \le n < N+g \end{cases}. \tag{4-1}$$

The matrix form of the data part of the transmitted symbol is

$$\mathbf{x}' = \mathbf{I}_u \mathbf{F}^H \mathbf{X}, \tag{4-2}$$

where $\mathbf{x}$ is the original data part of the transmitted symbol, the N by N matrix $\mathbf{I}_u$ is

$$\mathbf{I}_u = \begin{bmatrix} 0 & \cdots & \underset{\substack{uth \\ \downarrow}}{1} & 0 & \cdots \\ 0 & \cdots & & 1 & \cdots \\ \vdots & & & & \\ \cdots & 1 & & & 0 \end{bmatrix}, \tag{4-3}$$

and the IFFT matrix is

$$\mathbf{F} = \frac{1}{\sqrt{N}} \begin{bmatrix} 1 & 1 & \cdots & 1 \\ 1 & W & \cdots & W^{N-1} \\ \vdots & \vdots & \ddots & \vdots \\ 1 & W^{N-1} & \cdots & W^{(N-1)^2} \end{bmatrix}_{N \times N}. \tag{4-4}$$

Without symbol timing offsets and the CFO, the output sequence after FFT will be given by

$$\mathbf{Y} = \mathbf{F}\mathbf{I}_U\mathbf{F}^H\mathbf{X}. \tag{4-5}$$

The above equation can be further simplified as

$$\mathbf{Y} = \begin{bmatrix} 1 & 0 & \cdots & 0 \\ 0 & \omega & \cdots & 0 \\ \vdots & \vdots & \ddots & \vdots \\ 0 & 0 & \cdots & \omega^{(N-1)^2} \end{bmatrix}_{N \times N} \mathbf{X}. \tag{4-6}$$

As can be seen, the orthogonality among the subcarriers will not be affected. Instead, this intentionally introduced cyclic shift will result in a phase rotation of $e^{j2\pi un/N}$

($n = 1, \cdots N$) at the n th subcarrier in the receiver after FFT. In pilot based coherent modulation systems, this phase rotation can be compensated for by a frequency-domain channel equalizer [9-11].

As a result, we can cyclically shift or rotate the OFDM symbol after IFFT and assign the CP in such a way to improve the performance of the joint ML estimator [5].

According to last chapter, the performance of the joint estimator [5] for symbol timing and frequency offset in OFDM systems will improve if the energy of the CP is increased. Based on this observation, the transmitted signal will have a better synchronization performance if we rotate or shift the OFDM symbol to give rise to a higher energy CP for the symbol.

4.2 Implementation of the new data rotation scheme

Figs. 4.1 to 4.3 show how the new data rotation scheme can be implemented in an OFDM system. The parameters chosen are the same as those in the IEEE 802.11a standard [27]. Also, the timing and frequency offset are set to be 30, and 0.1, respectively. Fig. 4.1 and Fig. 4.2 show the block diagram of the new data rotation scheme in the transmitter and the receiver respectively. Fig. 4.3 shows the waveforms of a typical OFDM symbol before IFFT, after IFFT, after using the new data rotation scheme in the transmitter, after FFT in the receiver and after the rotation recovery, respectively.

As illustrated, the new data rotation scheme presents a new approach to detect the unknown synchronization parameters while maintaining the orthogonality among the subcarriers in an OFDM symbol. For a given OFDM symbol, this new approach involves

finding a maximum energy CP among N possible CPs (part of data block which consists of g data samples). After using the new data rotation scheme, the transmitted OFDM signal will not be white Guassian and has statistics that is different from the original system [5-25]. We will analyze the new data rotation scheme in the next section using order statistics theory [28-30].

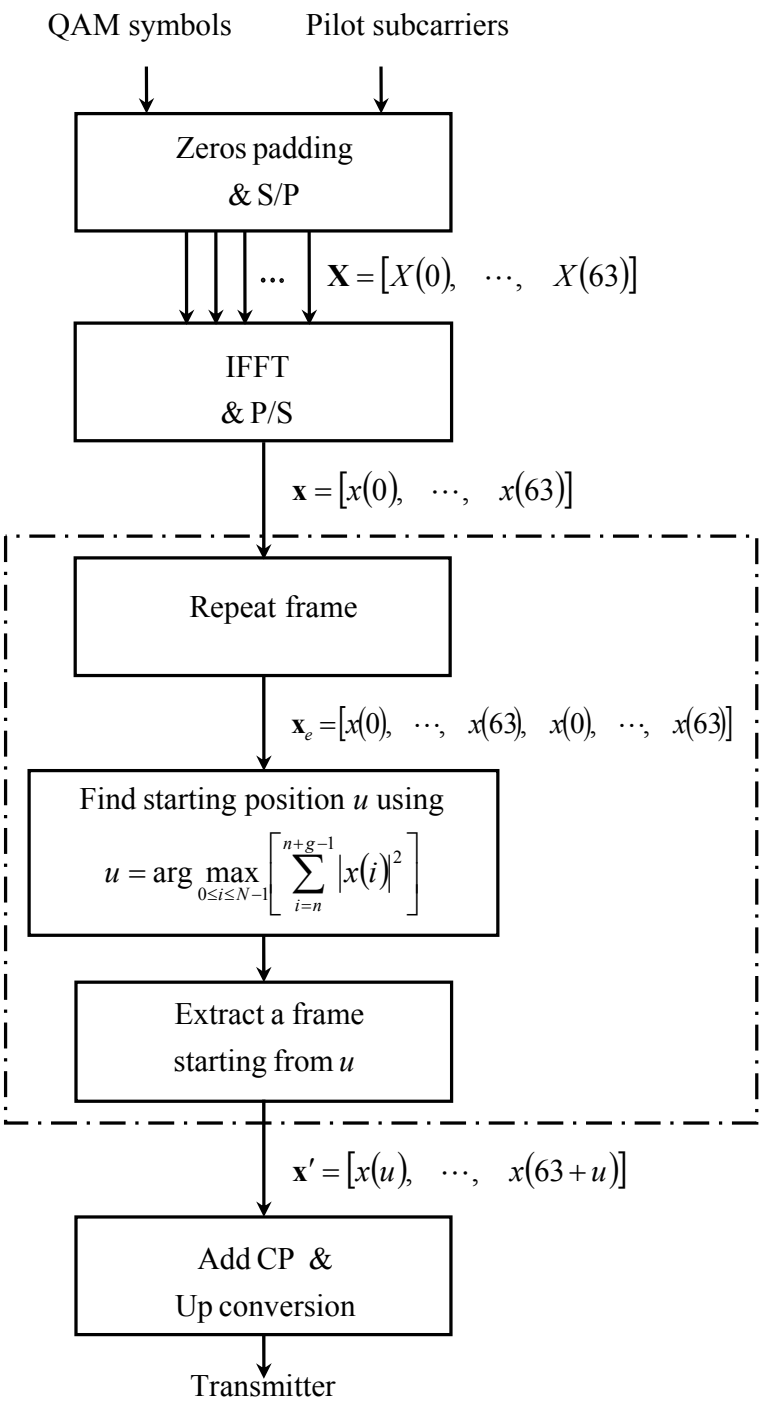

Fig. 4.1 Block diagram of new data rotation scheme in the transmitter.

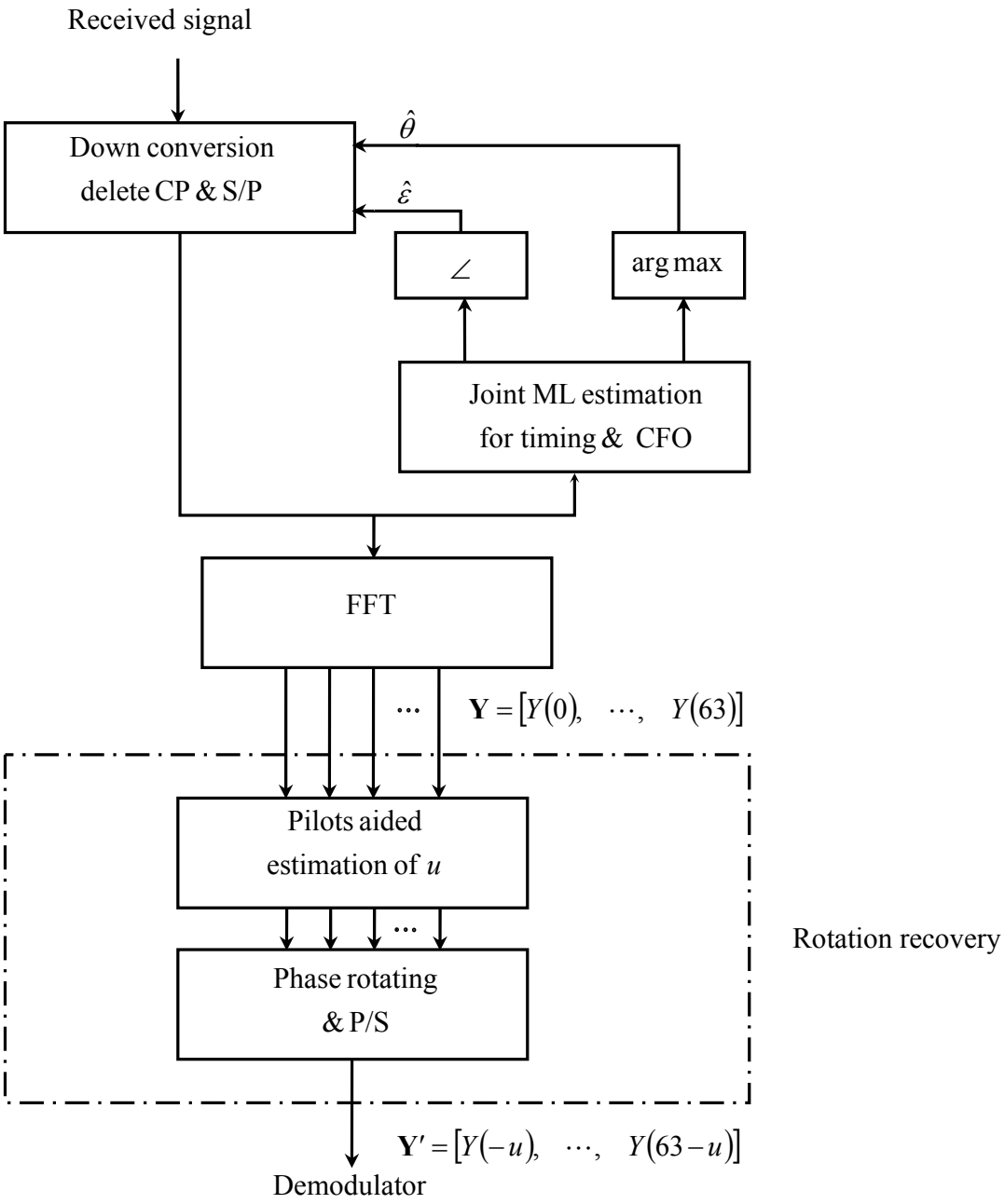

Fig. 4.2 Block diagram of new data rotation scheme in the receiver.

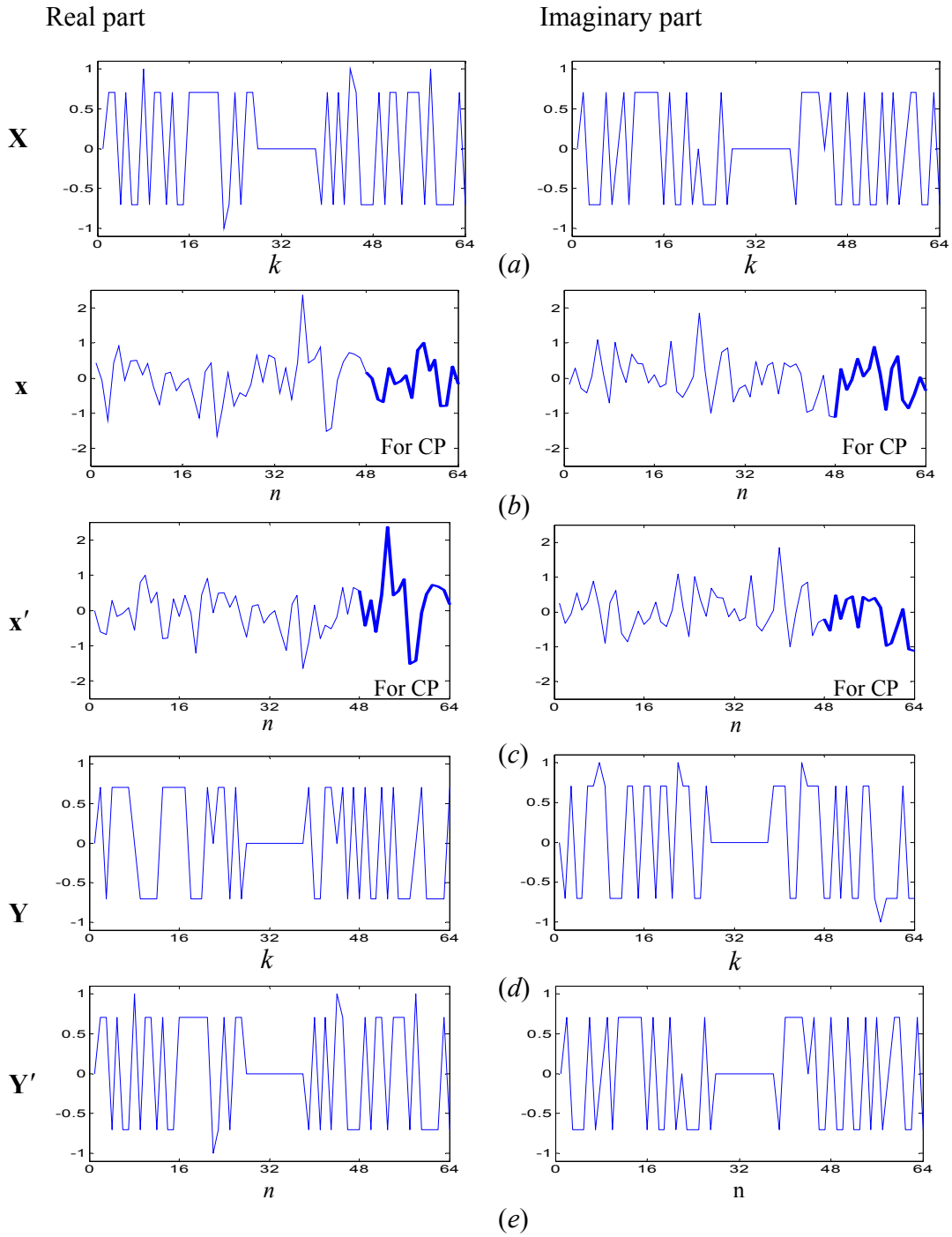

Fig.4.3 Waveforms of a typical OFDM symbol (a) before IFFT (b) after IFFT (c) after using the new data rotation scheme in the transmitter (d) after FFT in the receiver (e) after the rotation recovery.

4.3 An alternative way to recover the cyclic shift

According to (4-6), for a cyclic shift of u samples, the k th subcarrier experiences a phase shift of $e^{-j2\pi un/N}$. In case of coherent PSK modulation, we will employ FDE scheme to recover the random cyclic shift u. To give an accurate estimation of u, in IEEE802.11a standard, it is suggested that we inserted known pilot subcarriers.

However, if differential PSK modulation is employed across the subcarriers of the same OFDM symbol, the detrimental effect of the time synchronization error can be greatly reduced. This is due to the fact that adjacent subcarriers in the differential case experience a constant phase shift of $e^{-j2\pi un/N}$ irrespective of subcarrier position within the OFDM symbol.

By way of example, Fig. 4.4 (a) shows the received differential QPSK constellation for an OFDM system with cyclic shift $u = 5$, under perfect channel conditions. For comparison, the received QPSK constellation in coherent systems is also given in Fig. 4.4 (b). As can be seen, in (a), each subcarrier will rotate the same phase, while in (b), the phase for each subcarrier is increasing with the index of the subcarrier.

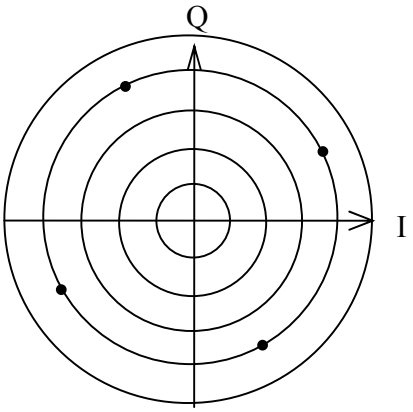

(a)

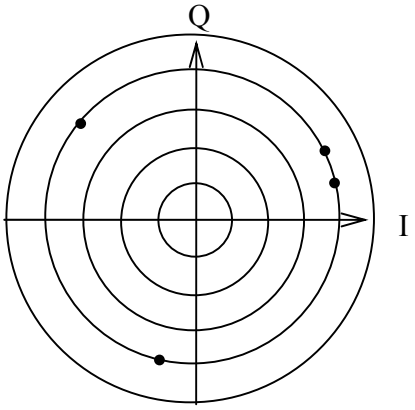

(b)

Fig 4.4 Constellation of (a) differential QPSK symbols and (b) coherent QPSK symbols under perfect channel conditions.

Chapter 5

Analysis of the New Data Rotation Scheme

In this chapter, we will investigate the new data rotation scheme. First, we give the analysis of the CFO estimator by applying the order statistics. A closed form of the SNR improvement is also given. Then, we investigate the expectation of the timing metric of the joint ML estimator. The improvement of its expectation value is presented.

5.1 Analysis of the CFO estimator

For a given OFDM symbol, we denote the energy of g successive samples that start from $n = v$ as η_v:

$$\eta_v = \sum_{i=v}^{v-g+1} |x(i)|^2 \ , \ 0 \le v \le N-1 \, , \tag{5-1}$$

where $x(0), \cdots, x(N-1)$ are the data samples after IFFT, and $x(N), \cdots, x(N-g+1)$ will be taken as $x(0), \cdots, x(g-1),$ respectively, in the case of $i \ge N$.

In [5], $x(0), \cdots, x(N-1)$ are approximated as complex Gaussian random variables (RVs) whose real and imaginary parts are independent and identically Gaussian

distributed with mean zero and variance $\sigma_s^2/2$. Consequently, from (5-1), $\eta_0, \cdots, \eta_{N-1}$ are identically χ^2 distributed. The mean and variance of η_v, $0 \le v \le N-1$ are given by

$$\mathrm{E}(\eta_v) = g\sigma_s^2 , \tag{5-2}$$

and

$$\mathrm{E}\left[(\eta_v - E[\eta_v])^2\right] = 2g\sigma_s^2 , \tag{5-3}$$

respectively.

Mathematically, the new data rotation scheme is to find the index of the maximum value of $\eta_0, \cdots, \eta_{N-1}$ given by

$$\eta_{\max} = \max\{\eta_0, \quad \cdots, \quad \eta_{N-1}\}. \tag{5-4}$$

Due to the overlap of data samples when summing over g data samples, $\eta_0, \cdots, \eta_{N-1}$ are not independent. Based on the fact that η_i and η_j have $(g - |i-j|)$ samples in common when $|i-j| < g$, the correlation between η_i and η_j $(0 \le i, j \le N-1)$ is given by

$$\mathrm{E}[\eta_i \eta_j] = \begin{cases} 2(g - |i-j|)\sigma_s^2, & |i-j| < g \\ 0, & \text{otherwise} \end{cases}. \tag{5-5}$$

From (5-2), the covariance matrix of $\eta_0, \cdots, \eta_{N-1}$ is given by

$$\mathbf{R} = \mathrm{E}\left[\left(\eta_0 - g\sigma_s^{\,2}, \quad \cdots, \quad \eta_{N-1} - g\sigma_s^{\,2}\right)\left(\eta_0 - g\sigma_s^{\,2}, \quad \cdots, \quad \eta_{N-1} - g\sigma_s^{\,2}\right)^{\mathrm{T}}\right], \tag{5-6}$$

where $(\bullet)^{\mathrm{T}}$ denotes transpose. Substituting (5-5) into (5-6), we get

$$\mathbf{R} = \begin{bmatrix} g\sigma_s^{\,2} & (g-1)\sigma_s^{\,2} & \cdots & \sigma_s^{\,2} & 0 & \cdots \\ (g-1)\sigma_s^{\,2} & g\sigma_s^{\,2} & \cdots & 0 & \cdots & \\ \vdots & \vdots & & & & \\ \sigma_s^{\,2} & 0 & & \ddots & & \\ 0 & \vdots & & & & \\ \vdots & & & & & g\sigma_s^{\,2} \end{bmatrix}. \tag{5-7}$$

In the original estimator, the energy of the CP, η_{N-g}, is χ^2 distributed with mean and variance given by (5-2) and (5-3), respectively. After using the new data rotation scheme, the energy of the CP is the maximum of $\eta_0, \cdots, \eta_{N-1}$ or that of (5-4). Hence, there is an increase in the energy of the CP after using the new data rotation scheme. From (5-2), the increase in the energy of the CP is given by

$$\Delta_{\mathrm{CP}}^{\,2} = \frac{\mathrm{E}[\eta_{\max}]}{\mathrm{E}[\eta_{N-g}]} = \frac{\mathrm{E}[\eta_{\max}]}{g\sigma_s^{\,2}}. \tag{5-8}$$

The derivation of the exact value of $\mathrm{E}[\eta_{\max}]$ is an intractable task. To obtain an approximate value of $\mathrm{E}[\eta_{\max}]$, we will now make two approximations. First, since the degree of freedom for the χ^2-distributed $\eta_0, \cdots, \eta_{N-1}$ is $2g$ and g is usually a large number, $\eta_0, \cdots, \eta_{N-1}$ can be well approximated as Gaussian distributed RVs. Second, we can ignore the dependence of $\eta_0, \cdots, \eta_{N-1}$. Specifically, from order statistics theory in

[28-30], the dependence of $\eta_0, \cdots, \eta_{N-1}$ can be neglected when $N >> g$, which is generally the case in OFDM systems.

After the above approximations, $\eta_0, \cdots, \eta_{N-1}$ are N independent and identically Gaussian distributed RVs with cumulative distribution function (cdf) $F_v(\eta)$ given by

$$F_v(\eta) = \int_{-\infty}^{\eta} \frac{e^{\frac{-\left(x-g\sigma_s^2\right)^2}{4g\sigma_s^4}}}{2\sigma_s\sqrt{g\pi}} dx, \; v = 0, \cdots, N-1. \tag{5-9}$$

From (5-4) and due to the independence of $\eta_0, \cdots, \eta_{N-1}$, the cdf of $\eta_{\max}$ are given by [28]

$$F_{\max}(\eta) = \Pr\{\eta_v \le \eta_{\max}, v = 0, \cdots, N-1\} = F_v(\eta)^N. \tag{5-10}$$

After some algebraic manipulations, $\mathrm{E}[\eta_{\max}]$ is then given by

$$\mathrm{E}[\eta_{\max}] = \int_{-\infty}^{\infty} N\eta \left[\int_{-\infty}^{\eta} \frac{e^{\frac{-\left(x-g\sigma_s^2\right)^2}{4g\sigma_s^4}}}{2\sigma_s\sqrt{g\pi}} dx\right]^{N-1} d\left[\int_{-\infty}^{\eta} \frac{e^{\frac{-\left(x-g\sigma_s^2\right)^2}{4g\sigma_s^4}}}{2\sigma_s\sqrt{g\pi}} dx\right]. \tag{5-11}$$

We will now show how the increase in the energy of the CP as given by Δ_{CP}^2 is related to the gain in the performance of the CFO estimator [5].

With a perfect knowledge of the timing offset, we get

$$\mathrm{E}[\gamma(\theta)] = \mathrm{E}[\gamma(\theta_0)]. \tag{5-12}$$

From (3-6), $\gamma(\theta_0)$ corresponds to the energy of the CP or given by η_{N-g}. In [6], the mean square error (MSE) of the CFO estimator is given by

$$\mathrm{var}(\hat{\varepsilon}_{\mathrm{old}}|\theta_0) = \frac{\left(\sigma_s^{\,2} + \sigma_w^{\,2}\right)^2 - \sigma_s^{\,4}}{(2\pi)^2 \sigma_s^{\,2} \mathrm{E}[\gamma(\theta)]}. \tag{5-13}$$

After the new data rotation scheme, the energy of the CP is the maximum of $\eta_0, \cdots, \eta_{N-1}$ or that of (5-4). Without considering the change in the statistics of the transmitted signal and substituting (5-8) into (5-13), the MSE of the CFO estimator after using the new data rotation scheme is given by

$$\mathrm{var}(\hat{\varepsilon}_{\mathrm{new}}|\theta_0) = \frac{\left(\sigma_w^{\,2} + \sigma_s^{\,2}\right)^2 - \sigma_s^{\,4}}{(2\pi)^2 \sigma_s^{\,4} g \Delta_{\mathrm{CP}}^{\,2}}. \tag{5-14}$$

From (5-2), the reduction in variance of the CFO estimator is given by

$$\frac{\mathrm{var}(\hat{\varepsilon}_{\mathrm{old}}|\theta_0)}{\mathrm{var}(\hat{\varepsilon}_{\mathrm{new}}|\theta_0)} = \Delta_{\mathrm{CP}}^{\,2}, \tag{5-15}$$

which corresponds to the increase in the energy of the CP.

The performance of the new scheme can also be characterized in another meaningful way. Specifically, using the original scheme, an SNR $\kappa = \sigma_s^{\,2}/\sigma_w^{\,2}$ will lead to a MSE of the CFO given by (5-13). For the same variance, a lower SNR of κ/κ_g would be needed if the new scheme is used and this can be obtained from (5-14).

Basically, κ_g represents a gain in SNR if the new scheme is used. Using (5-13) and (5-14) and after some manipulations,

$$\kappa_g = \Delta_{\mathrm{CP}} \sqrt{\frac{\kappa^2}{\Delta_{\mathrm{CP}}{}^2} + 2\kappa + 1} - \kappa . \tag{5-16}$$

The derivative of (5-16) with respect to κ is

$$\frac{\partial \kappa_g}{\partial \kappa} = \frac{\Delta_{\mathrm{CP}} + \dfrac{\kappa}{\Delta_{\mathrm{CP}}}}{\sqrt{\left(\Delta_{\mathrm{CP}} + \dfrac{\kappa}{\Delta_{\mathrm{CP}}}\right)^2 + 1 - \Delta_{\mathrm{CP}}{}^2}} - 1 . \tag{5-17}$$

Since $\Delta_{\mathrm{CP}}{}^2 > 1$, the RHS of (5-17) is larger than zero. Hence, κ_g is a monotone increasing function of κ. Specifically, when $\kappa = 1$, the SNR gain is

$$\kappa_g = \sqrt{3\Delta_{\mathrm{CP}}{}^2 + 1} - 1 . \tag{5-18}$$

For infinitely large input SNR κ, we get

$$\lim_{\kappa \to \infty} \kappa_g = \Delta_{\mathrm{CP}}{}^2 . \tag{5-19}$$

Clearly, the SNR gain κ_g increases as the input SNR κ increases, and has a maximum value equal to the increase in the energy of the CP $\Delta_{\mathrm{CP}}{}^2$.

5.2 Analysis of the symbol timing estimator

The symbol timing recovery relies on searching for a maximum output of the cost function given by (3-3). Note that θ is the time index corresponding to the first sample in the first window of g samples. This window slides along in time as the receiver searches for the start of the CP of an OFDM symbol. Denote the output of the cost function $f(\theta)$ as timing metric. Fig. 5.1 shows this timing metric with respect to the time index θ averaging over 2000 OFDM symbols.

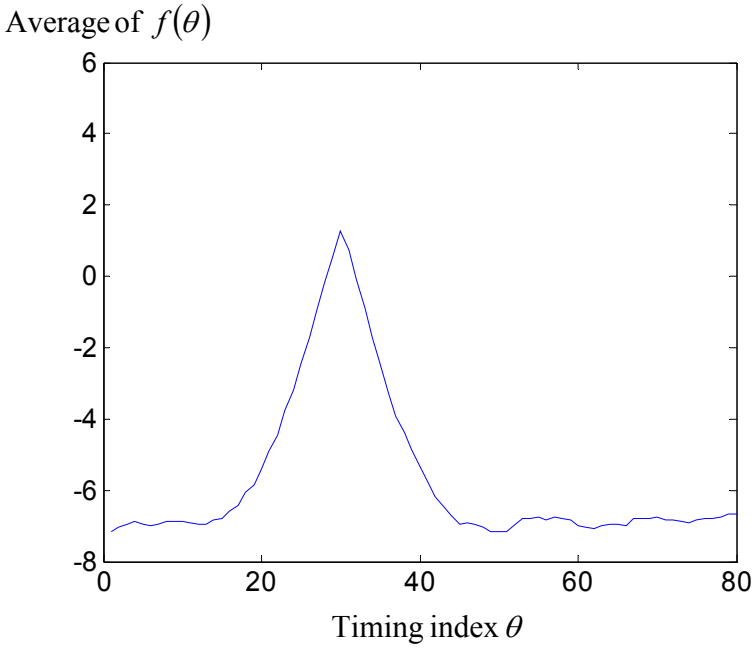

Fig. 5.1 Average of timing metric $f(\theta)$ using Beek's scheme.

According to the analysis given in Chapter 3, the timing errors are most likely to occur around the correct start position. Since the received signal is made up of a signal and a noise component, (3-5) can be rewritten as

$$f(\theta)=\left|\sum_{n=\theta}^{\theta+g-1} r(n)r^{*}(n+N)\right|-\rho\left[\sum_{n=\theta}^{\theta+g-1}|r(n)|^{2}+|r(n+N)|^{2}\right]. \tag{5-20}$$

Taking $\rho \approx \frac{1}{2}$ when the SNR is high, and ignoring the second order term due to the noise, the above equation can be given by

$$f(\theta)=\sum_{n=\theta}^{\theta+g-1}\frac{\left[|s(n)|-|s(n+N)|\right]^{2}}{2} + inPhase_{2\pi\varepsilon}\left[s(n)w^{*}(n+N)+s^{*}(n+N)w(n)\right]-\mathrm{Re}\left[s(n)w(n)+s(n+N)w(n+N)\right], \tag{5-21}$$

where inPhase$\{.\}$ means the component in the $2\pi\varepsilon$ direction. The quadrature part is neglected because the Rician distribution can be approximated by a Gaussian when taking the envelope of a dominant signal with Gaussian noise. Note that the first term of (5-21) is comprised of the modular difference of the samples in two timing windows. Hence, when $\theta=\theta_0$, the timing metric $f(\theta)$ is Gaussian distributed with mean zero. When $\theta=\theta_0$, assuming that the timing metric $f(\theta)$ is still Gaussian distributed, the mean of $f(\theta)$ is given by

$$\mathrm{E}\left[f(\theta)\right]=\sum_{n=\theta}^{\theta}\frac{\left(|s(n)|-|s(n+N)|\right)^{2}}{2}. \tag{5-22}$$

Specifically,

$$\mathrm{E}[f(\theta)]=\begin{cases}\sum_{n=\theta}^{\theta+g-1}\frac{\left(|s(n)|-|s(n+N)|\right)^2}{2}, & \theta<\theta_0-g+1\\ \sum_{n=\theta}^{\theta_0-g+1}\frac{\left(|s(n)|-|s(n+N)|\right)^2}{2}, & \theta_0-g+1\le\theta<\theta_0\\ 0, & \theta=\theta_0\\ \sum_{n=\theta}^{\theta_0+g-1}\frac{\left(|s(n)|-|s(n+N)|\right)^2}{2}, & \theta_0<\theta\le\theta_0+g-1\\ \sum_{n=\theta}^{\theta+g-1}\frac{\left(|s(n)|-|s(n+N)|\right)^2}{2}, & \theta<\theta_0+g-1\end{cases}. \tag{5-23}$$

When SNR is high and the variance of the timing metric $f(\theta)$ is small, the performance of the symbol timing estimator will depend on the mean of $f(\theta)$.

As for Beek's scheme, assuming that the signal is Gaussian distributed and independent, the above equation is given by

$$\mathrm{E}[f(\theta)]=\begin{cases}-g\sigma_s^{\,2}, & |\theta-\theta_0|>g\\ -\left(g-|\theta-\theta_0|\right)\sigma_s^{\,2}, & g\ge|\theta-\theta_0|>0\\ 0, & \theta=\theta_0\end{cases}. \tag{5-24}$$

By using the new data rotation scheme, the modular difference of $s(n)$ and $s(n+N)$ will increase. Note that either $s(n)$ or $s(n+N)$ is inside of the CP or its copies of the data segment. According to the appendix B, the mean of $f(\theta)$ is given by

$$\mathrm{E}[f(\theta)]=\begin{cases}-g\Delta_{\mathrm{CP}}^{\,2}\sigma_s^{\,2}, & |\theta-\theta_0|>g\\ -\left(g-|\theta-\theta_0|\right)\Delta_{\mathrm{CP}}^{\,2}\sigma_s^{\,2}, & g\ge|\theta-\theta_0|>0\\ 0, & \theta=\theta_0\end{cases}. \tag{5-25}$$

As shown in Fig. 5.2, the average timing metric after using the new data rotation scheme is more acute than that of the old scheme as shown in Fig. 5.1.

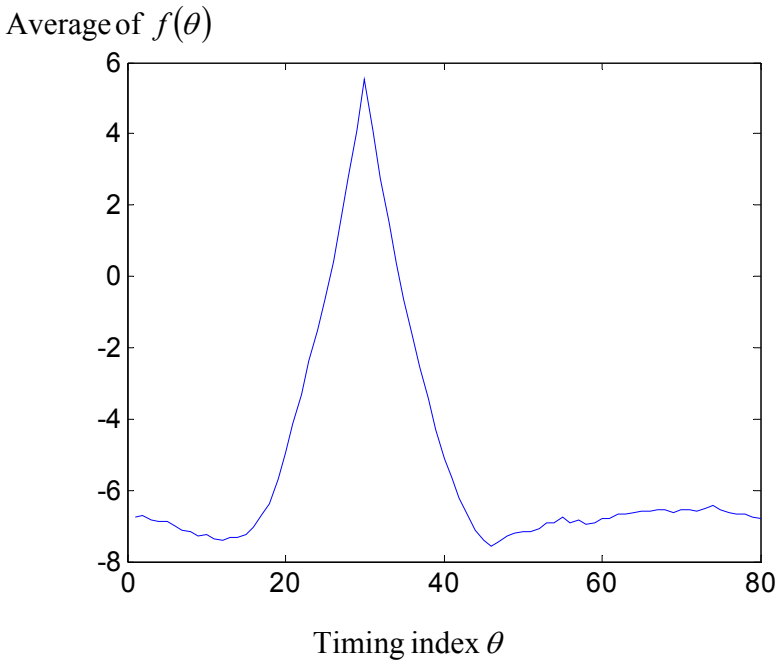

Fig. 5.2 Average of timing metric $f(\theta)$ after using new data rotation scheme.

Chapter 6

Simulation Results

To show the theoretical analysis in the previous chapter, we will present some simulation results to validate the theoretical results obtained and to illustrate the performance of the new data rotation scheme. The simulation parameters chosen are the same as those in the IEEE 802.11a standard [27]. More specifically, $N = 64$, $g = 16$, $\theta_0 = 30$, and $\varepsilon = 0.1$.

6.1 Simulation to prove the theoretical analysis

First, to show that the approximations we made to obtain (5-8) in Chapter 5 are at least fairly accurate, Fig.6.1 shows the relationship between the relative error of the approximation given by (5-8) relative to the value obtained from simulation at various N for $g = 16$. As can be seen, the approximation is quite accurate, especially when the ratio of N/g is large.

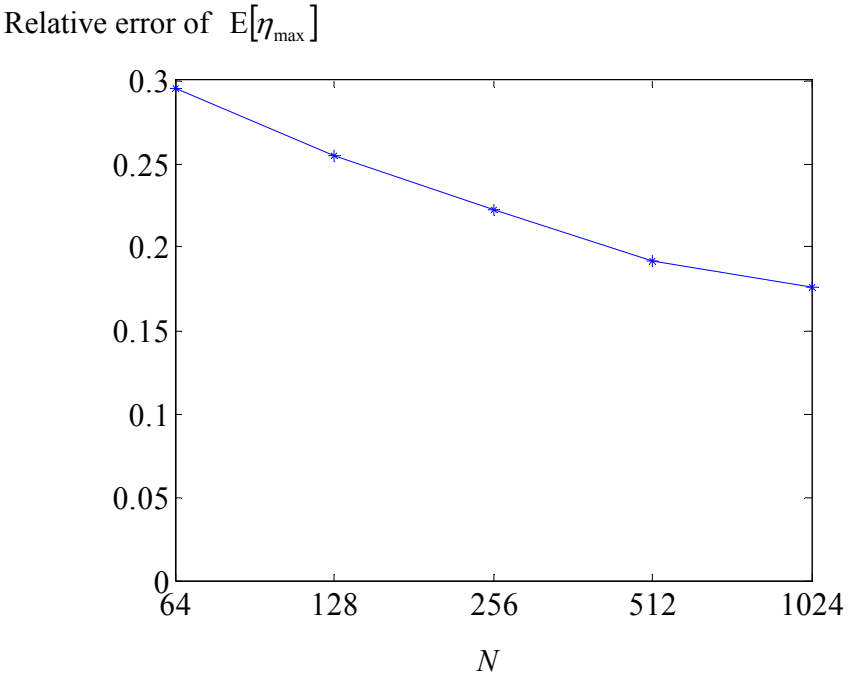

Fig. 6.1 Relative error of $\mathrm{E}[\eta_{\max}]$ versus the FFT size N at $g = 16$.

We will now proceed to verify the SNR gain given by (5-18) in section V. Specifically, with $N = 64$ and $g = 16$ and thus $\Delta_{\mathrm{CP}}{}^2 = 1.6$ dB, Fig. 6.2 (a) shows the theoretical analysis (solid curve) and the simulation results (star mark) of the SNR gain Δ_{SNR} as a function of the input SNR κ. The relatively small difference between the analysis and the simulation result is due to the change in the statistics of the transmitted signal. As shown in Fig.6.2 (b), without the effect of the timing offset, the performance gain of the CFO estimator by using the new data rotation scheme is almost the same for all SNR.

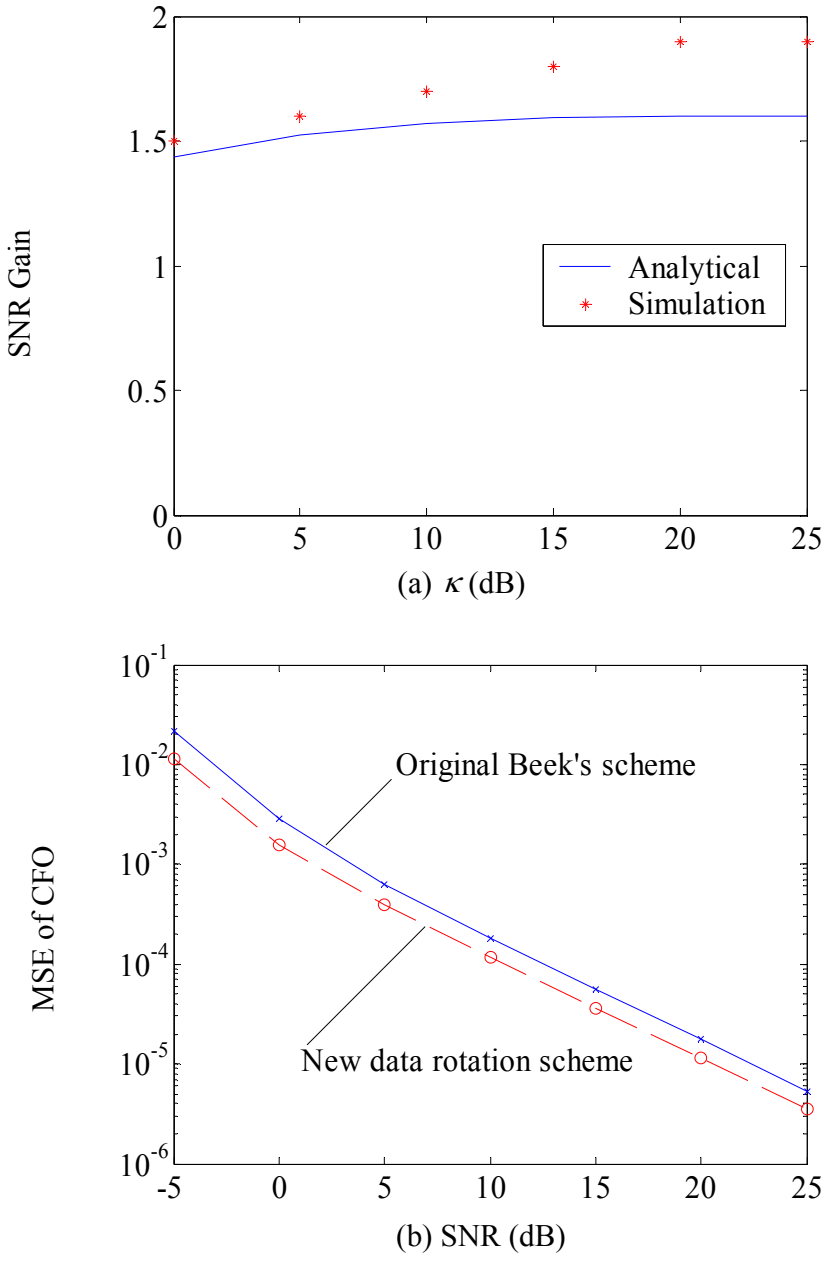

Fig. 6.2 (a) Simulation and analytical results of SNR gain versus the input SNR and (b) performance of CFO estimator without the timing offset.

6.2 Performance of the new data rotation scheme

Lastly, Fig.6.3 compares the performance of the new data rotation scheme and the original Beek's scheme. The simulation is done using 10,000 runs. The solid line represents the performance of the original and the new data rotation scheme while the dashed line gives the performance of the original scheme with a 1.6 dB gain.

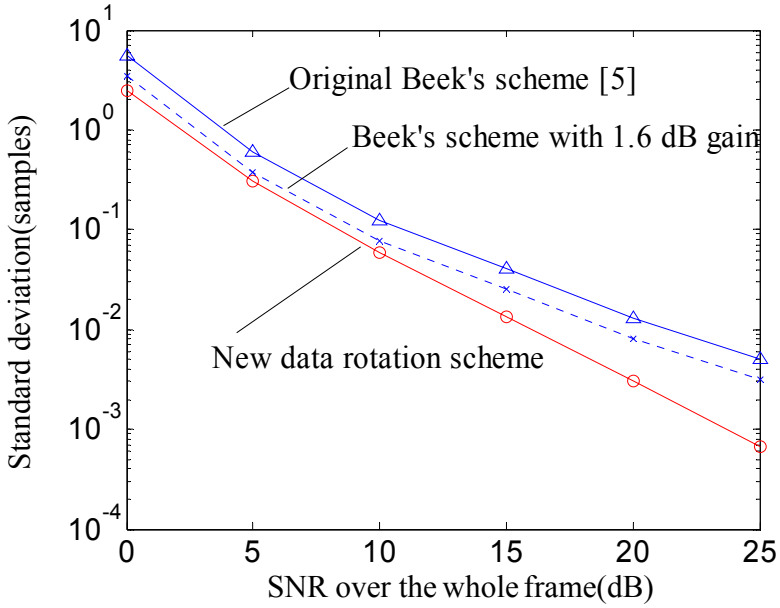

(a) Performance of timing estimator

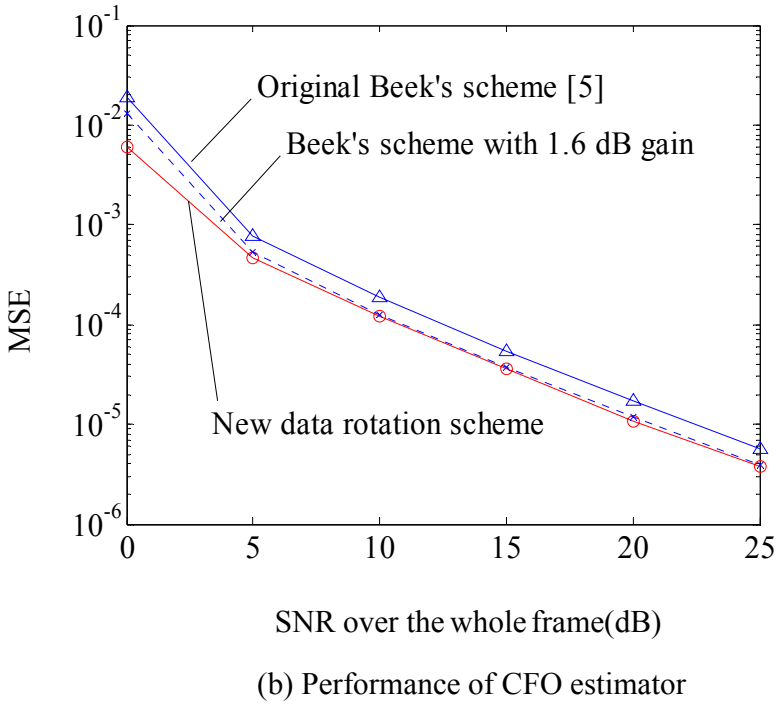

(b) Performance of CFO estimator

Fig. 6.3 Comparison of joint timing and CFO estimation using the new data rotation scheme with the original Beek's scheme [5].

As can be seen, the performance of the new data rotation scheme surpasses that of the joint ML estimation proposed by Beek [5]. As for the timing estimator, the new data rotation scheme gives a much better result at high SNR. Specifically, a gain of 6dB can be obtained when $SNR = 15$ dB. For the frequency offset estimator, the MSE of the frequency offset is reduced by about 1.6 dB for almost all SNR. Since a larger deviation in the timing offset propagates to the CFO estimator [6], the reduction in the timing offset errors by using the new data rotation scheme will lead to a better performance of the CFO estimator at low SNR.

Chapter 7

Conclusions and Future Works

In this Chapter, we conclude this thesis and propose some future work using this new data rotation scheme.

7.1 Conclusions

We have proposed a new data rotation scheme for the joint timing and CFO estimation of OFDM systems. The new data rotation scheme cyclically rotates the CP of each transmitted OFDM symbols to provide a higher energy CP. Significant performance improvement can be obtained in both timing and CFO estimation. Theoretical and simulation results show that the performance gain in the CFO estimator is independent of SNR and is equal to the increase in the energy of the CP. Specifically, the new scheme can provide a 1.6 dB gain in the performance of the CFO estimator and a 6dB gain for the timing estimator at 15dB SNR.

7.2 Future Works

The new data rotation scheme can give rise to a better synchronization result with the trade off of increasing the whole energy of the transmitted signal. Besides, since the

signal samples are dependent in an OFDM symbol, the autocorrelation of the transmitted signal is no longer stationary.

To overcome this non-stationary characteristic of the power spectrum density (PSD) of the transmitted signal, we will consider applying this scheme in the space-time coded OFDM systems. Hence, for each OFDM system, we allocate the CP into different position of the symbol to make the whole energy of the transmitted signal stationary. In the receiver with the known knowledge of this CP location, the difference in the CP location for each transmit antenna will not affect the synchronization estimation.

Besides the synchronization problems we mentioned, the new data rotation scheme can also be used in another field of study in OFDM systems, the reduction of the high peak factor of the modulated signal. This instantaneous to the mean power ratio is usually called as the PAPR. Since the high power samples are usually inside the CP of the OFDM symbol, by using a controllable voltage position, the new data rotation scheme we proposed will lead to considerable gains in the reduction of PAPR.

References

[1] R. W. Chang, “Synthesis of Band-limited Orthogonal Signal for Multichannel Data Transmission,” *Bell Syst. Tech. J.,* vol. 45, pp. 1775-1796, Dec. 1966.

[2] S. B. Weinstein and P. M. Ebert, “Data Transmission by Frequency Division Multiplexing using the Discrete Fourier Transform,” *IEEE Trans. Commun.,* vol. COM-19, no. 5, pp. 628-634, Oct. 1971.

[3] Perter Smulders, “Exploting the 60 GHz Band for Local Wireless Multimedia Access: Prospects and Future Directions,” *IEEE Communications Magazine*, pp. 140-147, Jan. 2002.

[4] J. A. C. Bingham, “Multicarrier Modulation for Data Transmission: An Idea Whose Time Has Come,” *IEEE Communications Magazine*, pp. 5-14, May 1990.

[5] Jan Jaap van de Beek, “ML Estimation of Time and Frequency Offset in OFDM Systems,” *IEEE Trans. Signal Processing*., vol. 45, pp. 1800-1805, July. 1997.

[6] Navid Lashkarian, “Class of Cyclic Based Estimation for Frequency Offset Estimation of OFDM Systems,” *IEEE Trans. Commun*., vol. 48, pp. 2139-2149, Dec. 2000.

[7] Rohit Negi and John M. Cioffi, “Blind OFDM Symbol Synchronization in ISI channels,” *IEEE Trans. Commun*., vol. 50, pp. 1525-1534, Sept. 2002.

[8] Helmut Bölcskei, “Blind Estimation of Symbol Timing and Carrier Frequency Offset in Wireless OFDM Systems,” *IEEE Trans. Commun*., vol. 49, pp. 988-999, June 2001.

[9] Karthik Ramasubramanian, Kevin Baum, "An OFDM Timing Recovery Scheme with Inherent Delay-Spread Estimation," *IEEE Trans. on Signal Processing,* vol. 45, no. 7, pp. 3111-3115, July, 2001.

[10] Zhongzhe Xiao and Zaiwang Dong, "Improved GIB Synchronization Method for OFDM Systems," *IEEE ICT*, vol. 2, pp. 1417-1421, 2003.

[11] Lei Xu, Zaiwang Dong, "A New GIB Frequency Synchronization Algorithm with Reduced Influence of ISI for OFDM Systems," *IEEE 2002 International Conference on Communications, Circuits and Systems and West Sino Expositions*, vol. 1, pp. 129-133, 2002.

[12] Baoguo Yang, Khaled Ben Letaief, Roger S. Cheng, and Zhigang Cao, "Timing Recovery for OFDM Transmission," *IEEE J. Select. Areas Commun*., vol. 50, pp. 2278-2291, Nov. 2000.

[13] Michael Speth, Ferdinand Classen and Heinrich Mcyr, "Frame synchronization of OFDM systems in frequency selective fading channels," *IEEE Vehicular Technology Conferece*, vol. 3, pp. 1807-1811, May 1997.

[14] Yasamin Mostofi, Donald C. Cox and Ahmad Bahai, "Effect of Frame Synchronization Errors on Pilot-aided Channel Estimation in OFDM: Analysis and Solution," *Wireless Personal Maultimedia Communications*, vol. 3, pp. 1309-1313, 2002.

[15] H. Minn, M. Zeng, and V. K. Bhargava, "On Timing Offset Estimation for OFDM Systems," *IEEE Commun. Letter,* vol. 4, no. 7, pp. 242-244, July 2000.

[16] P. Moose, "A Technique for Frequency and Timing Synchronization for OFDM," *IEEE Trans. Comm.,* vol. 45, no. 12, pp. 1613-1621, Dec. 1997.

[17] T. Schmidl Cox, "Robust Frequency and Timing Synchronization for OFDM," *IEEE Trans. Comm.,* vol. 45, no. 12, pp. 1613-1621, Dec. 1997.

[18] K. J. Bang, N. S. Cho, J. H. Cho, K. C. Kim, H. C. Park, and D. S. Hong, "A Coarse Frequency Offset Estimation in an OFDM System Using the Concept of the Coherence Phase Bandwidth," *IEEE ICC2000,* New Orleans, pp. 1135-1139, June 2000.

[19] K. Taura *et al.*, "A Digital Audio Broadcasting (DAB) Receiver," *IEEE Trans. Consumer Electronics,* vol. 42, no. 3, pp. 322-327, Aug. 1996.

[20] I. H. Hwang, H. S. Lee, and K. W. Kang, "Frequency and Timing Period Offset Estimation Technique for OFDM Systems," *IEEE Electron. Letter,* vol. 34, no. 6, pp. 520-521, Mar. 1998.

[21] M. Luise and R. Reggiannini, "Carrier Frequency Acquisition and Tracking for OFDM Systems," *IEEE Trans. Commun.,* vol. 44, no. 1, pp. 1590-1598, Nov. 1996.

[22] K. W. Kang, J. Ann, and H. S. Lee, "Decision-directed Maximum-Likelihood Estimation of OFDM Frame Synchronization Offset," *IEEE Electron. Letter,* vol. 30, no. 25, pp. 2153-2154, Dec. 1994.

[23] Jian Sun, Issa, H. M. A. and Pediang Qiu, "Frequency and Timing Synchronization and Channel Estimation in Preamble Based OFDM System," *IEEE 2002 International Conference on Communications, Circuits and Systems and West Sino Expositions*, vol. 2, pp. 1063-1068, 2002.

[24] Yuping Zhao and Sven-Gustav Haggman, "Intercarrier Interference Self-Cancellation Scheme for OFDM Mobile Communication Systems," *IEEE Trans. Commun.,* vol. 49, no. 7, pp. 1185-1191, July 2001.

[25] Ufuk Tureli, Didem Kivanc, and Hui Liu, "Experimental and Analytical Studies on a High-resolution OFDM Carrier Frequency Offset Estimator," *IEEE Trans. Vehicular Tchnol.,* vol. 50, no. 2, pp. 629-643, March. 2001.

[26] J. G. Proakis, "Digital Communications,"4th ed: McGraw-Hill, 2001.

[27] IEEE 802.11, "Draft Supplement to Standard for Telecommunications and Information Exchange between Systems LAN/MAN Specific Requirements-part 11: Wireless MAC and PHY Specifications: High Speed Physical Layer in the 5 GHz Band," *Tech*., May 1999.

[28] David and John M. Cioffi, "Order Statistics,"2nd ed. New York: Wiley, 1981.

[29] Biyi Afonja, "The Moments of the Maximum of Correlated Normal and t -Variates," *Journal of the Royal Statistical Society. Series B (Methodological)*, vol. 34, pp. 251-262, 1972.

[30] G. S. Watson, "Extreme Values in Samples from m -Dependent Stationary Stochastic Processes," *Annals of Mathematical Statistics*, vol. 25, pp. 798-800, Dec. 1954.

APPENDIX A The timing error of $+1$ and -1 Sample

According to (3-3), a timing error of $+1$ sample occurs when $\chi_{\theta_0+1} > 0$, where χ_{θ_0+1} is

$$\chi_{\theta_0+1} = |\gamma(\theta_0+1)| - |\gamma(\theta_0)| - \rho[\phi(\theta_0+1) - \phi(\theta_0)]. \tag{A-1}$$

Using (3-5) and (3-6), we have

$$\begin{aligned}\chi_{\theta_0+1} = &-\left|\sum_{m=\theta_0}^{\theta_0+g-1} r(m)r^*(m+N)\right| + \left|\sum_{m=\theta_0+1}^{\theta_0+g} r(m)r^*(m+N)\right| \\ &+ \rho\left[|r(\theta_0)|^2 + |r(\theta_0+N)|^2 - |r(\theta_0+g)|^2 - |r(\theta_0+g+N)|^2\right]\end{aligned} \tag{A-2}$$

From (2-3) and (3-3), when $\theta_0 \le n \le \theta_0 + g - 1$, $r(n)$ is inside the cyclic prefix and is correlated with $r(n+N)$. They can be represented by

$$r(n) = s'(n-\theta_0) + w(n) \tag{A-3}$$

and

$$r(n+N) = s'(n-\theta_0)e^{j2\pi\varepsilon} + w(n+N), \tag{A-4}$$

where, due to the phase shift introduced by the CFO ε,

$$s'(n) = s(n)e^{j\psi_0 + \frac{j2\pi n\varepsilon}{N}}, \tag{A-5}$$

and ψ_0 is the initial phase shift.

Substituting (A-3), (A-4) and (A-5) into the first term on the right hand side of (A-2), we get

$$\left|\sum_{m=\theta_0}^{\theta_0+g-1} r(m)r^*(m+N)\right| = \left|\sum_{m=0}^{g-1}|s(m)|^2 + w'_{sw} + w'_{ww}\right|, \tag{A-6}$$

where

$$w'_{sw} = \sum_{m=\theta_0}^{\theta_0+g-1} e^{j2\pi\varepsilon}\left\{w(m)[s'(m-\theta_0+N)]^* + w^*(m+N)s'(m-\theta_0)\right\} \tag{A-7}$$

and

$$w'_{ww} = \sum_{m=\theta_0}^{\theta_0+g-1} e^{j2\pi\varepsilon} w(m)w^*(m+N). \tag{A-8}$$

The modulus square of (A-6) is

$$\left|\sum_{m=0}^{g-1}|s(m)|^2 + w'_{sw} + w'_{ww}\right|^2 = \left[\sum_{m=0}^{g-1}|s(m)|^2 + \mathrm{Re}(w'_{sw} + w'_{ww})\right]^2 + [\mathrm{Im}(w'_{sw} + w'_{ww})]^2. \tag{A-9}$$

When the SNR is high, the noise term w'_{ww}, and the second term $[\mathrm{Im}(w'_{sw} + w'_{ww})]^2$ on the right hand side (RHS) of (A-6) can be ignored compared with the first term. Then, (A-9) becomes

$$\left|\sum_{m=0}^{g-1}|s(m)|^2 + w'_{sw} + w'_{ww}\right|^2 = \left\{\sum_{m=0}^{g-1}|s(m)|^2 + \mathrm{Re}(w'_{sw})\right\}^2. \tag{A-10}$$

Square rooting (A-10), and taking the energy of the cyclic prefix to be larger than the noise term $\mathrm{Re}(w'_{sw})$, we can rewrite (A-6) as

$$\left|\sum_{m=\theta_0}^{\theta_0+g-1} r(m)r^*(m+N)\right| = \sum_{m=0}^{g-1}|s(m)|^2 + \mathrm{Re}(w'_{sw}). \tag{A-11}$$

The second term on the RHS of (A-2) is given by

$$\left|\sum_{m=\theta_0+1}^{\theta_0+g} r(m)r^*(m+N)\right| = \left|s(g)s^*(N+g) + \sum_{m=1}^{g-1}|s(m)|^2 + w''_{sw}\right|. \tag{A-12}$$

When the SNR is high and the length of the cyclic prefix g is large enough, we can assume that

$$\sum_{m=1}^{g-1}|s(m)|^2 > \mathrm{Re}(w''_{sw}) + \mathrm{Re}\left[s(g)s^*(N+g)\right]. \tag{A-13}$$

Hence, using the same approach as for deriving (A-11), the second term on the RHS of (A-2) can be approximated as

$$\left|\sum_{m=\theta_0+1}^{\theta_0+g} r(m)r^*(m+N)\right| = \mathrm{Re}\left[s(g)s^*(N+g)\right] + \sum_{m=1}^{g-1}|s(m)|^2 + \mathrm{Re}(w''_{sw}). \tag{A-14}$$

By ignoring the second order term due to the noise, the factors inside the third term on the RHS of (A-2) are given by

$$|r(\theta_0)|^2 + |r(\theta_0+N)|^2 - |r(\theta_0+g)|^2 - |r(\theta_0+g+N)|^2 = 2|s(0)|^2 - |s(g)|^2 - |s(N+g)|^2 + w'''_{sw}, \tag{A-15}$$

where

$$w'''_{sw} = 2\mathrm{Re}\left[w^*(\theta_0)s'(0) + e^{j2\pi\varepsilon}w^*(\theta_0+N)s'(0) - w^*(\theta_0+g)s'(g) - w^*(\theta_0+N+g)s'(N+g)\right]. \tag{A-16}$$

Using

$$\mathrm{Re}\left[s(g)s^*(N+g)\right]-\frac{1}{2}|s(g)|^2-\frac{1}{2}|s(N+g)|^2=\frac{1}{2}|s(g)-s(N+g)|^2, \tag{A-17}$$

taking $\rho\approx\frac{1}{2}$ when the SNR is high, and substituting (A-11), (A-14) and (A-15) into (A-2), χ_{θ_0+1} is given by

$$\chi_{\theta_0+1}=-\frac{1}{2}|s_+-v_+|^2+\frac{1}{2}|v_+|^2, \tag{A-18}$$

where

$$s_+=s(g)-s(N+g) \tag{A-19}$$

and

$$v_+=e^{j\psi_0}\left[w^*(\theta_0+g)-e^{j2\pi\varepsilon}w^*(\theta_0+g+N)\right]. \tag{A-20}$$

From (A-18), χ_{θ_0+1} will depend on s_+, that is, the difference between $s(g)$ and $s(N+g)$.

Similarly, as for the error of -1 sample, χ_{θ_0-1} is given by

$$\chi_{\theta_0-1}=-\frac{1}{2}|s_--v_-|^2+\frac{1}{2}|v_-|^2, \tag{A-21}$$

where

$$s_-=s(-1)-s(N-1) \tag{A-22}$$

and

$$v_{-} = e^{j\psi_0}\left[w^*(\theta_0 - 1) - e^{j2\pi\varepsilon} w^*(\theta_0 + N - 1)\right] . \quad \text{(A-23)}$$

APPENDIX B Proof of $\mathrm{E}\left[\left|s_{\pm}\right|^2\right] = \frac{\Delta_{\mathrm{CP}}{}^2(N-2g)+N}{N-g}\sigma_s{}^2$

From (3-11) and (3-15), assuming that the transmitted signal is independent of the noise in the receiver and the noise is AWGN, the expectation of χ_{θ_0+1} and χ_{θ_0-1} are given by

$$\mathrm{E}\left[\chi_{\theta_0+1}\right] = -\frac{\mathrm{E}\left[\left|s_{+}\right|^2\right]}{2} \tag{B-1}$$

and

$$\mathrm{E}\left[\chi_{\theta_0-1}\right] = -\frac{\mathrm{E}\left[\left|s_{-}\right|^2\right]}{2}\ , \tag{B-2}$$

respectively.

From (3-18) and assuming that $s(N+g)$ and $s(g)$ are independent, the modulus square of s_+ in the RHS of (B-1) can be given by

$$\mathrm{E}\left[\left|s_{+}\right|^2\right] = \mathrm{E}\left[\left|s_{N+g}\right|^2\right] + \mathrm{E}\left[\left|s_{g}\right|^2\right]. \tag{B-3}$$

According to Fig. 3.2, $s(N+g)$ is inside the CP of the current OFDM symbol, while $s(g)$ is outside the CP.

Since the average power of the OFDM data block is $\sigma_s{}^2$, the energy of the CP corresponding to the last g samples of the OFDM data block is $\Delta_{\mathrm{CP}}{}^2 g\sigma_s{}^2$. The average power of the CP $\sigma_{\mathrm{CP}}{}^2$ is

$${\sigma_{\mathrm{CP}}}^2 = {\Delta_{\mathrm{CP}}}^2{\sigma_s}^2 . \tag{B-4}$$

Consequently, since the energy of the whole data block is fixed, the average power of the rest $(N-g)$ samples, denoted by ${\sigma_{\mathrm{data}}}^2$, is given by

$${\sigma_{\mathrm{data}}}^2 = \frac{(N-g{\Delta_{\mathrm{CP}}}^2)}{N-g}{\sigma_s}^2 . \tag{B-5}$$

Substituting (B-4) and (B-5) into (B-3), we get

$$\mathrm{E}\left[\left|s_{+}\right|^2\right] = \frac{{\Delta_{\mathrm{CP}}}^2(N-2g)+N}{N-g}{\sigma_s}^2 . \tag{B-6}$$

Similarly, as for the error of -1 sample, $\mathrm{E}\left[\left|s_{-}\right|^2\right]$ is given by

$$\mathrm{E}\left[\left|s_{-}\right|^2\right] = \frac{{\Delta_{\mathrm{CP}}}^2(N-2g)+N}{N-g}{\sigma_s}^2 . \tag{B-7}$$

This completes the proof.

Publication List

1. Ko Chi Chung and Shi Miao, “A New Data Rotation Scheme To Improve the ML Synchronization Schemes used in OFDM Systems”, submitted to IEEE Trans. on Wireless Communications.
2. Shi Miao and Ko Chi Chung, “A New Data Rotation Scheme To Improve the ML Synchronization Schemes used in OFDM Systems”, IEEE ICICS-PCM, 2003.
3. Shi Miao, “Complete ML mapping for timing estimates in CP based synchronization schemes”, IEEE Communication Theory Workshop, 2003.